UPPSALA
UNIVERSITET

Digital Comprehensive Summaries of Uppsala Dissertations from the Faculty of Science and Technology 670

Computational Studies of Nanotube Growth, Nanoclusters and Cathode Materials for Batteries

PETER LARSSON

ACTA
UNIVERSITATIS
UPSALIENSIS
UPPSALA
2009

ISSN 1651-6214
ISBN 978-91-554-7603-8
urn:nbn:se:uu:diva-108261

Dissertation presented at Uppsala University to be publicly examined in Polhemsalen, Ångströmlaboratoriet, Uppsala, Friday, October 23, 2009 at 13:15 for the degree of Doctor of Philosophy. The examination will be conducted in English.

Abstract

Larsson, P. 2009. Computational Studies of Nanotube Growth, Nanoclusters and Cathode Materials for Batteries. Acta Universitatis Upsaliensis. *Digital Comprehensive Summaries of Uppsala Dissertations from the Faculty of Science and Technology* 670. 59 pp. Uppsala. ISBN 978-91-554-7603-8.

Density functional theory has been used to investigate cathode materials for rechargeable batteries, carbon nanotube interactions with catalyst particles and transition metal catalyzed hydrogen release in magnesium hydride nanoclusters.

An effort has been made to the understand structural and electrochemical properties of lithium iron silicate (Li_2FeSiO_4) and its manganese-doped analogue. Starting from the X-ray measurements, the crystal structure of Li_2FeSiO_4 was refined, and several metastable phases of partially delithiated Li_2FeSiO_4 were identified. There are signs that manganese doping leads to structural instability and that lithium extraction beyond 50% capacity only occurs at impractically high potentials in the new material.

The chemical interaction energies of single-walled carbon nanotubes and nanoclusters were calculated. It is found that the interaction needs to be strong enough to compete with the energy gained by detaching the nanotubes and forming closed ends with carbon caps. This represents a new criterion for determining catalyst metal suitability. The stability of isolated carbon nanotube fragments were also studied, and it is argued that chirality selection during growth is best achieved by exploiting the much wider energy span of open-ended carbon nanotube fragments.

Magnesium hydride nanoclusters were doped with transition metals Ti, V, Fe, and Ni. The resulting changes in hydrogen desorption energies from the surface were calculated, and the associated changes in the cluster structures reveal that the transition metals not only lower the desorption energy of hydrogen, but also seem to work as proposed in the gateway hypothesis of transition metal catalysis.

Keywords: Materials science, density functional theory, cathode materials, hydrogen-storage materials, carbon nanotube growth

Peter Larsson, Department of Physics and Materials Science, Materials Theory, Box 530, Uppsala University, SE-75121 Uppsala, Sweden

ISSN 1651-6214
ISBN 978-91-554-7603-8
urn:nbn:se:uu:diva-108261 (http://urn.kb.se/resolve?urn=urn:nbn:se:uu:diva-108261)

To my family

List of Papers

This thesis is based on the following papers, which are referred to in the text by their Roman numerals.

I **An ab initio study of the Li-ion battery cathode material Li_2FeSiO_4**
Peter Larsson, Rajeev Ahuja, Anton Nytén and John O. Thomas
Electrochemistry Communications **8**, 797-800 (2006)

II **Structural and electrochemical aspects of Mn-substitution into Li_2FeSiO_4 from DFT calculations**
Peter Larsson, Rajeev Ahuja, Anti Liivat and John O. Thomas
Submitted manuscript

III **Structural, magnetic, and energetic properties of Na_2FePO_4F, Li_2FePO_4F, $NaFePO_4F$, and $LiFePO_4F$ from ab initio calculations**
M. Ramzan, S. Lebègue, P. Larsson and R. Ahuja
Journal of Applied Physics **106**, 043510 (2009)

IV **Calculating carbon nanotube-catalyst adhesion strengths**
Peter Larsson, J. Andreas Larsson, Rajeev Ahuja, Feng Ding, Boris I. Yakobson, Haiming Duan, Arne Rosén and Kim Bolton
Physical Review B **75**, 115419 (2007)

V **The Importance of Strong Carbon-Metal Adhesion for Catalytic Nucleation of Single-Walled Carbon Nanotubes**
Feng Ding, Peter Larsson, J. Andreas Larsson, Rajeev Ahuja, Haiming Duan, Arne Rosén and Kim Bolton
Nano Letters **8**, 463-468 (2008)

VI **On the Stability of Single-Walled Carbon Nanotubes and Their Growing Ends**
Jakub D. Baran, Wojciech Kołodziejczyk, Peter Larsson, Rajeev Ahuja and Andreas Larsson
Submitted manuscript

VII **Copper/Molybdenum Nanocomposite Particles as Catalysts for the Growth of Bamboo-Structured Carbon Nanotubes**
Zhonglai Li, J. Andreas Larsson, Peter Larsson, Rajeev Ahuja, Joseph M. Tobin, Justin O'Byrne, Michael A. Morris, Gary Attard and Justin

D. Holmes
Journal of Physical Chemistry C **112**,12201-12206 (2008)

VIII **Role of Catalysts in Dehydrogenation of MgH_2 Nanoclusters**
Peter Larsson, C. Moysés Araújo, J. Andreas Larsson, Puru Jena and Rajeev Ahuja
Proc. Natl. Acad. Sci. USA (PNAS) **105**, 8227-8231 (2008)

The following papers are co-authored by me, but are not included in the Thesis.

- **Measuring Pancharatnam's relative phase for SO(3) evolutions using spin polarimetry**
  Peter Larsson and Erik Sjöqvist
  Physical Review A **68**, 042109 (2003)

- **Noncyclic mixed state phase in SU(2) polarimetry**
  Peter Larsson and Erik Sjöqvist
  Physics Letters A **315**, 12-15 (2003)

Reprints were made with permission from the publishers.

Contents

1. Introduction

The general background of the work in this thesis may be seen as one of current topics of today: how to rebuild our energy and transportation infrastructure. The primary energy solution now is based on the combustion of various fossil fuels such as coal, oil, and natural gas. There is an increasing awareness that the current production of fossil fuels cannot be sustained forever (i.e. "peak oil"), and that the resulting pollution is affecting the environment in a variety of unsustainable ways. It is envisioned that the current technology will be replaced by electricity from renewable energy sources, and that the electricity would drive electric engines and fuel cells. How to do this is, in fact, known in principle. Both the electric engine and the fuel cell are old, well-established technologies, and likewise, generating electricity by hydropower, solar power, wave power etc is being routinely done today. What it comes down to, however, is scale and cost-effectiveness. All these solutions work today, but need to become smaller, stronger, faster, and most importantly, cheaper, in order to compete with existing technologies. This is not only important to preemptively outcompete fossil fuels, but also to ease the transition, because it is likely that the transition will need to be done rapidly once a peak oil scenario happens.

It is at this stage that materials science comes in, because many of the engineering problems in energy storage and production become inherently connected to materials properties when pursuing higher technical efficiency. For example, one can build perfectly fine electric vehicles with Li-ion batteries of the same kind as is used in cell phones and computers, but the cost becomes unreasonable, mainly due to expensive elements used in the cathode materials in the battery cells. What is needed is cheaper battery cathodes. Another example is storing hydrogen gas for feeding a fuel cell. We can do this easily by compressing hydrogen gas and putting it in steel tank under high pressure, but this solution is very uncompetitive compared to a plastic tank filled with gasoline (the gravimetric energy density of gasoline is about 44 MJ/kg vs 6 MJ/kg for a complete liquid hydrogen system). There are also obvious safety issues with having hydrogen gas in a vehicle. To compare favorably with a fossil fuel, one must store the hydrogen chemically bound in a solid state. This is an active field of material science research, because so far no material has been found that is both light enough and able to release hydrogen gas under reasonable thermodynamical conditions.

A trend in materials research has been the move towards nanostructured systems, meaning that the materials are tuned at the nanometer, or even down to the atomic scale, to improve technical properties. A typical example is

nanosized powders that consists of particles of only 100-1000 atoms. Such powders often have enhanced chemical reactivity both due to the high surface area, and changes in chemical and physical properties due to quantum mechanical size confinement effects. Another example is nanometer scaled devices, consisting of nanostructures like carbon nanotubes. Working at this microscopic level is practically very hard, samples are delicate, and noise comes into measurements. The advancement of experimental methods such as thin film deposition and atomic force microscopy has been very important to provide tools to scientist and engineers to realize and investigate new kinds of materials. But much knowledge has also been gained by theoretical physics and chemistry. This field has developed rapidly during the last 50 years and moved from traditional theoretical approaches based on observing, writing (approximate) differential equations, and then solving for some special cases, to a full-fledged virtual laboratory where matter in a wide range of conditions can be studied in a controlled environment. Of course, that this was possible in principle has been known ever since the discovery of quantum mechanics, but it is the recent explosion in computational power and development of new approximate methods that has made ab initio study (no fitting of models to experimental data) of chemistry and physics practically possible.

The ab initio approach to materials science has been used in this thesis to investigate and predict properties of several materials and chemical reactions related to energy and nano-energineering applications. The outline of the thesis is as follows: first an overview and discussion of the computational methods used is given in chapter 2, which is then followed by a summary of the papers in chapter 3. The first three papers are related to cathode materials for rechargable batteries. Papers IV-VII focus on catalysis and growth of carbon nanotubes. The last paper (VIII) presents a theoretical investigation of transition metal catalyzed hydrogen release in magnesium nanoclusters.

The work on rechargeable batteries has focused on characterizing new alternative cathode materials with regards to structural and electrochemical properties. It was also important to compare the outcome of the theroretical calculations to experiments to establish whether the existing methods (density functional theory) would be sufficiently accurate to model the materials. In paper I, the lithium iron silicate material is investigated. It is found that the structure refined from X-ray measurements is probably suboptimal, and that several phases of partially delithiated lithium iron silicate may exist. In paper II, the low limit of manganese substitution in the material is probed for signs of higher electrochemical capacity. Unfortunately, indications of structural instability are found, and deintercalation beyond 50% still occurs at too high potentials for practical use (4.7-4.8 V).

Carbon nanotubes are a fascinating building material for atomic scale engineering. But the particular applications usually rely on having nanotubes with a specific diameter or chirality. This is a big problem, because so far, tight control of the products of carbon nanotube synthesis has not been achieved. The work on catalysis of carbon nanotube growth presented here started by investigating models for how to study the interaction of carbon nanotubes with

the metal catalysts used during synthesis. The main finding was that the commonly used approach of having a single metallic atom at the tube end was not accurate enough. The minimum acceptable arrangement was a ring of metal atoms at the tube end. With such a model, trends and overall binding energies were reasonably accurate. Once knowledge was gained on how to model the interaction, two groups of metals were investigated: known efficient catalysts of growth and classic catalysts that one might hope would work, but in practice does not (Pd, Au, Cu). It was found that efficient catalysts shared an important property, viz. having binding energies to the carbon nanotube in the medium range. In paper V, it is argued that this is because carbon-metal interaction must balance two forces: being strong enough to attach the catalyst to the nanotube (to continue growth and catalysis) and being weak enough to release carbon atoms from the surface to be incorporated into the growing tube.

In the later work on carbon nanotube growth, the conditions for achieving chirality selective growth was investigated. It is argued that bottom up synthesis, for example by small fragment seeding or surface design is unlikely to achieve sufficiently selectivity due to the closeness in energy of carbon nanotubes. Instead, higher selectivity can be achieved by selecting growing nanotube fragments by their binding strengths to the surface and/or stability when dissociated from the metal particle surface.

In addition to the two themes on batteries and nanotubes mentioned above, a study on MgH_2 clusters is reported in paper VIII. Magnesium hydride is a much studied material in the context of solid state hydrogen storage. It is known that addition of small amounts of transition metals to nanocrystalline magnesium powders can significantly increase the hydrogen release/uptake speed. In the paper, it is demonstrated how the transition metal atoms Ti, V, Fe, and Ni not only lower the surface desorption energies of hydrogen significantly, but also continue to bind hydrogen atoms even when the hydrogen content of the cluster decreases. It is observed, through geometry relaxations, that Fe migrates from the surface sites to the interior sites during the dehydrogenation process. These observations confirm, at the atomic level, the gateway/shuttling hypothesis of transition metal catalysis in magnesium powders.

2. Methods & Approximations

This section is intended to provide extra information about computational methods to aid reproduction, justify the different technical approaches chosen, and give some account of the accuracy of the employed methods, rather than being an exposition of density functional theory and its numerical implementation.

2.1 The choice of theory

There are two fundamental ways of studying the chemical and physical properties of system of atoms. One either constructs a model containing free parameters and tries to fit it to experimental data, or one mounts a brute-force attack and tries to determine the eigenfunctions and eigenvalues by solving the Schrödinger equation, or a similar relativistic equation. This approach is mostly parameter-free, and is known as a first-principles, or ab initio, calculation. Its main drawback is an exponential, or greater, increase in computational expense, as the number of atoms and electrons increases. In practice, only small molecules can be studied with full precision in this way.

A priori, an ab initio approach would be preferable if within available computational constraints. Therefore, all papers included in the thesis contain calculations based on density functional theory[1, 2] – an approximate ab initio method. Semi-empirical and/or parametrized force-fields could not be used here because the goal in many of the papers was to predict trends related to changes in chemical bonds (which is what one usually parametrizes, in order to predict e.g. structure and phase transitions). In retrospective, though, such methods might still have been useful in an initial stage to perform a more exhaustive search of possible geometries.

The only ab initio methods that can routinely be used for the simulation sizes considered here (big clusters, and doped supercells with >100 atoms) are standard Hartree-Fock, 2nd order Møller-Plesset perturbation theory (MP2), and density functional theory (DFT). Others, like coupled-cluster, higher-order perturbation theory, and quantum Monte Carlo are too computationally expensive, especially considering the computational facilities available five years ago, when the work in this thesis was started. Recently, the situation has improved, with methods such as GW approximation[3] being included in the Vienna ab initio simulation package (VASP) [4–8], and the maturity of Monte Carlo-programs (e.g. CASINO[9]), together with an order of magnitude in-

crease in computational capacity at the Swedish national supercomputing centers.

The primary reason for choosing DFT is that even the simplest local density approximation to the exchange-correlation energy (see below) gives better chemistry than Hartree-Fock, and with generalized gradient approximations (GGA) such as PBE [10, 11], the predictions can surpass second order Møller-Plesset perturbation theory (MP2) wave functions, e.g. when calculating heats of formations[12, 13]. A secondary reason is that DFT is a well-developed method within the solid-state community, with robust protocols that are easily applied to periodic systems, such as crystals, especially in combination with a plane-wave basis set.

The most critical shortcoming of DFT, with regard to this work, became apparent when trying to describe highly oxidized states produced by lithium deintercalation in the cathode materials in Papers I-III. They contain transition metals bound to oxygen in tetrahedral or octahedral geometry, similar to many transition metal oxides. In that case, it was obvious that the chemistry of Fe/Mn-atoms cannot be described accurately with normal DFT, due to the to underestimation of intercalation voltages. The Li^+ binding in these materials is almost purely electrostatic and should be well represented by DFT; the error is instead in the change of the transition metal's oxidation state. When an electron is extracted from a localized 3d orbital of e.g. Fe, and transferred to the metallic 2s orbital of the Li^+ ion in the metal, it will experience much less self-interaction in the metallic state of lithium, producing an underestimation of the energy required for this redox process, and thus give an appearance of lower intercalation voltage. To try to diagnose the problem, a GGA+U treatment was used to simulate the effect of localized electrons. It did recover part of the missing voltage, but was ultimately of limited use for prediction of properties, because different model parameteres (U and J) are necessary to calculate the intercalation voltage over the cathode's complete lithium capacity range.

When it comes to metal clusters and nanotubes, previous DFT calculations on metal clusters and nanotubes (separately) have shown reasonably good agreement with experimental measurements of density of states and magnetic moments (see e.g. [14, 15]). Surprisingly, even transition metal-carbon dimers seem to be described properly[16], despite strong multireferential character in the case of Fe-C[17]. One can therefore expect to at least recover qualitative effects about carbon-metal interactions in the metal cluster–nanotube interface using DFT with the GGA approximation to the exchange-correlation potential.

Magnesium metal has been thoroughly investigated with DFT. Bulk properties of magnesium hcp metal were first calculated by Chou and Cohen[18], reproducing bulk properties with good agreement to experimental data. Later studies included investigations of the phase diagram and the hcp/bcc phase transition[19–21] – also with good agreement. There is very little experimental data available for small Mg clusters, so here it is more difficult to judge, but the DFT study by Köhn et al. seems to agree with mass spectrometry findings and quantum chemical calculations at the CCSD(T) level for Mg_4.

Bulk properties of MgH_2 has been studied with DFT previously, especially effects of allyoing[22–24], due to its importance as a hydrogen storage material. The agreement with available measurements is generally good, especially in capturing trends. A large computational study of potential hydrogen storage compounds, including Mg-based ones, were published recently[25]. There, the errors in enthalpies were estimated to be around 10 kJ/mol. This is a large error, compared to what is usually considered "chemical" accuracy, 1 kJ/mol, but still sufficiently accurate to detect substantial changes in e.g. hydrogen desorption energy, because the hydrogen desorption enthalpy for undoped MgH_2 is about 75 kJ/mol.

2.2 Born-Oppenheimer approximation

The Born-Oppenheimer approximation[26] was used in all calculations. It is a standard approximation in almost all modern theoretical approaches. Some even see it as a paradigm of chemistry, since it is the basis of fundamental concepts such as *molecule* and *crystal* (otherwise, the geometry of a system of atoms could only be described as a superposition of different geometries). The approximation consists of separating the wavefunction of the system into two independent parts: the electronic component and the nuclear component. It means that, in practice, the electronic wavefunction is solved for a set of fixed nuclei coordinates; one defines a fixed molecule or crystal based on the nuclei positions. The assumption here is that the electronic subsystem evolves adiabatically during nuclear motion, which is usually a very good approximation because of the great difference in speed between electrons and nuclei– the electronic state will immediately respond to any change in the nuclear position–so the nuclei will appear to be in rest from the point of view of the electrons.

As stated by R. G. Woolley [27]: *"The Born-Oppenheimer approximation is usually satisfactory for ground electronic states of neutral molecules [but] its failure in the excited electronic states of polyatomic molecules and ions is a common occurrence."* Some examples where the B-O approximation is problematic are hydrogen motion (the nuclei is very light), high impact collisions of atoms/ions onto surfaces (the velocity is high), charge-transfer reactions, and photochemical reactions (transitions between different potential energy surfaces). Also metals present difficulties because the validity of the B-O approximation rests on the assumption that there are no degenerate electronic levels.

Especially relevant to this thesis is the observed failure of the B-O approximation when trying to calculate Raman spectra of metallic nanotubes[28] and graphene[29] (although no such calculations have been performed in this work). In practice, however, B-O is a very good approach, again as judged by the excellent agreement with experiments that have been produced by B-O calculations[30–32]–even for metals[33, 34].

Some progress has been made in going beyond the B-O approximation: a perturbative approach exists, taking into account the diagonal Born-Oppenheimer correction[35–37], and full wavefunction calculations have been presented for the H_3 isotopomer[38], but it is still not possible to go beyond the B-O approximation for large systems due to the computational expense and lack of developed methodology.

2.3 DFT exchange-correlation approximation

When using DFT, the most critical choice is which approximation to the exchange-correlation potential to use. The starting approach here has always been the GGA approximations (generalized gradient approximation), by Perdew and Wang [39, 40]) or the similar PBE approximation by Perdew, Burke and Ernzerhof[10], which uses both the electron density, and its gradient to derive the exchange-correlation potential. This choice was motivated by the fact that hybrid functionals do not display universal performance over many different chemical systems. The fitting parameters of e.g. B3LYP are not well-adapted to large molecules and transition metals[41], as is studied here. In fact, as shown in a study by Delley[13], PBE (a GGA functional without fitted parameters) and B3LYP (a three-parameter hybrid functional) produce almost identical mean average deviations when calculating heats of formations over a large set of molecules (577 molecules and 15 atoms).

It is common, especially among physicists, to hear it being stated that GGA does not really improve upon the simple local density approximations, but this is not true over a sufficiently large range of materials. In the 577 molecule study mentioned above, the root-mean-square error of the formation enthalpies for the local density functional is 31 kJ/mol, while the corresponding value for PBE is 22 kJ/mol. Perdew and co-workers reached similar conclusions when comparing functionals for 18 different solids in [42]: average errors in lattice constants and bulk moduli were improved when going from LDA to PBE. The surface energy did worsen, but this error was corrected at the meta-GGA level.

Lately, some advances have been made in constructing approximations improving upon GGA for many classes of materials, such as TPSS[42]. The TPSS functional was used in the work on MgH_2 clusters, where it was suspected that surface effects might play an important role. A recent promising development for solids is AM05[43], which is as accurate as hybrid functionals for solids, but from an ab initio construction.

2.4 Treatment of relativistic effects

Relativistic effects generally start to significantly affect chemical properties when the constituent atoms are heavier than potassium (3d-metals and above).

Somewhere around lead (Z=82), nonrelativistic treatments cannot even be used in a qualitative way. In this work, inclusion of relativistic effects was especially important for the palladium and gold clusters used in the carbon nanotube studies. It can also be expected to be important, but not strictly necessary, for the battery cathode materials and magnesium clusters, because they were doped with 3d-metals.

Two different approaches was used to deal with relativistic effects. The scalar relativistic approximation was used in the calculations with VASP, where the mass-velocity and Darwin terms from the fully relativistic equations are included via perturbation theory into the Schrödinger equation, but the spin-orbit interactions are omitted. With this approach, the angular momentum quantum number and the spin quantum number remain good quantum numbers. In TURBOMOLE, scalar relativistic effects were included in an implicit way through effective core potentials ("pseudopotentials") derived from fully-relativistic calculations.

2.5 Method of Discretization

In order to solve the problem numerically, some type of discretization must be introduced, either by e.g. finite-differences, or an expansion of the wavefunction/Kohn-Sham orbitals into a finite basis set. The traditional way to do this for non-periodic systems has been the linear combination of atomic orbitals (LCAO) approach, usually employing an atom-centered Gaussian basis set. This approach was used for the MgH_2 clusters, and also for some of the SWNT-metal cluster energy calculations, but was only partially successful in the second case due to convergence problems and difficulties dealing with magnetism in the larger Fe, Co and Ni-clusters. The underlying cause was that the LCAO basis set is not suitable to describe metallic states, and that many quantum chemical programs are designed and optimized for dealing with molecules or small clusters, lacking robust algorithms for finding the optimal spin multiplicity.

It was much more fruitful to apply the same methods that were used to simulate periodic systems (crystals) in Papers I-III. A cluster can be simulated in such a framework by using a supercell approach, where the clusters are embedded in a supercell surrounded by vacuum in all directions. This allowed isolated clusters to be calculated with periodic boundary conditions using the projector-augmented wave-method (see below), and algorithms designed for magnetic metals could be employed in optimization of the spin state. It turned out that in practice, the slowdown from using the supercell approach with a much larger basis set was compensated by faster convergence of the electronic density and the spin state.

The projector-augmented wave-method (PAW)[44] might be seen as combination of the augmented plane wave and the pseudopotential approach. In essence, it is an all-electron method, but with frozen atomic cores. Its main advantage is that a full all-electron density is derived explicitly in each calcu-

lation, eliminating the transferability problems of pseudopotentials. Recently, a good review of the main ideas of PAW was published by Blöchl [45].

The fundamental idea in PAW is to solve an atomic problem with DFT using e.g. the Koelling-Harmon relativistic Hamiltonian[46] and then transform the full one-particle orbitals into smooth "auxiliary" orbitals that can be described with a relatively small plane wave basis set outside the core region. With the PAW transformation, any operator and expectation value can be transformed into acting only on the auxiliary orbitals, so that physical quantities such as total energy and spin can be evaluated purely from the auxiliary orbitals. The end result may be seen as doing pseudopotential calculations with dynamically fitted pseudopotentials. The most popular computer implementation of PAW is found in VASP, together with the highly regarded PAW transformations developed by G. Kresse and D. Joubert[8]. VASP was used for all periodic calculations included in this thesis. In general, the default PAW transformations were used in the calculations, except for sodium and lithium, where transformations with more valence electrons were used to better accomodate the fully ionized Li^+ and Na^+ states. This choice improved derived intercalation voltages for cathode materials by about 0.1 V.

The PAW method is generally seen as superior to using normal norm-conservering pseudopotentials or ultrasoft pseudopotentials. With awareness of the kind of PAW transformation used, the results of PAW are close to all-electron methods[47]. In practice, strictly chemical properties, which are mostly the focus in this thesis, are sufficiently well described with the PAW method, because they are mainly determined by valence electron properties. It might have been possible to use ultrasoft pseudopotentials, but it was avoided due to known problems with magnetic compounds[8] (e.g. Fe, which is present in both the metal clusters and the cathode materials). In VASP, the computational performance gains would also have been modest.

A further advantage of using PAW for molecules and clusters is that the basis set is to a large degree non-local, the plane-wave basis used for the auxiliary functions fills the whole simulation box, which eliminates most of the basis-set superposition error that might otherwise occur with an atomic-centered basis. What otherwise happens is that, when trying to calculate the binding energy of two molecules (such as a metallic cluster and a nanotube) in an incomplete basis, the two molecules share basis functions at the interface when the complex is calculated, which leads to an artificial lowering of the total energy and an overestimation of the binding energy.

2.6 Quality of basis sets

Once one, or several, discretization methods have been chosen, the numerical precision of the calculation will depend on the size and the flexibility of the basis set used (or the point density of the grid when using finite-differences). With a plane-wave based approach, like in the PAW method, this error is relatively easy to control. The number of plane waves in the basis set is usually

expressed as a kinetic energy cut-off – all plane waves up to this kinetic energy are included in the basis set – and the convergence of electronic properties with respect to this number is uniform.

The PAW transformations supplied with VASP come with a default recommended plane-wave energy cut-off, which usually is enough to deliver total energies converged to about 0.01 eV or 1 kJ/mol (even less if error cancellation is present, such as for chemical reactions). In practice, using this energy cut-off creates problem when doing volume relaxation of cells, because the diagonal components of the stress tensor is sensitive to the size of the basis set. The error manifests itself as an artificial compression of the system ("Pulay stress"), but can be avoided by using a sufficiently large basis set (normally +25-50% with respect to the default values). This approach was followed in Paper II, and has the additional advantage that all other properties, such as reaction energies, are very well converged. Otherwise, the normal way to determine cell volumes is to construct the equation of state from a set of fixed volume calculations, and determine the equilibrium volume from that. It gives a correct volume, even if a relatively small basis set is used, due to a fortunate error cancelation. That method was used in Paper I, III.

In contrast, Gaussian basis sets do not converge uniformly, unless designed specifically to have that behavior. Instead, they will tend to oscillate around the fully converged energy. The main determining factor of a Gaussian basis set's quality is the number of Gaussian basis functions used to describe each valence orbital ("doube zeta", "triple zeta" etc). In TURBOMOLE, the basis sets are abbreviated SVP, TZVP and QZVP for double zeta (split-valence), triple zeta valence + polarization functions, and quadruple zeta valence + polarization functions, respectively. These basis sets can be found in the EMSL basis set exchange[1], for use in other programs than TURBOMOLE.

The quality of a Gaussian basis set should always be checked by comparing energies and geometries at different levels, but as a rule of thumb, double zeta or split-valence is enough to capture trends ("qualitative"), triple zeta is sufficient for comparison with experimental results ("quantitative"), while quadruple zeta will approach the converged limit necessary for "benchmark" calculations. This rule of thumb applies to DFT only, wave function based methods may require a bigger basis set for the same level of precision. A translation between plane-wave and Gaussian basis sets are given in Table 2.1.

It is of course possible to construct one's own Gaussian basis set for a specific purpose, in order to speed up the calculations. This approach was used in the MgH_2 cluster work, where a magnesium basis set developed by Köhn et al.[48] was able to better describe the metallic state of the dehydronated clusters than the generic basis sets.

[1] `https://bse.pnl.gov/bse/portal`, use the search terms `Ahlrichs TZV`, `Ahlrichs Polarization` etc.

Table 2.1: *A outline of different basis sets of roughly equal precision and how they can be invoked in the* TURBOMOLE *and the* VASP *programs.* ζ *is a shorthand notation for the Gaussian basis function.*

Gaussian type	TURBOMOLE	VASP	Numerical precision
Double-ζ	`def-SVP`	`PREC=Low`	Qualitative
Triple-ζ	`def-TZVP`	`PREC=Medium`	Quantitative
Quadruple-ζ	`def-QZVP`	`PREC=High`	Benchmark

2.7 Periodicity and k-point sampling

In a calculation with periodic boundary conditions, such as crystals and vacuum-embedded clusters, eigenvalues and eigenstates must normally be calculated for every possible **k**-vector in the first Brillouin zone, to describe the energy dispersion of the bands. How many **k**-vectors that are actually necessary to get accurate energies and properties depends on the size of the cell, and the kind of system calculated. Molecules and clusters, by definition have no dispersions at all, and only one k-point (the gamma point) should be used, *even* if the vacuum layer is not sufficiently thick. The choice of only the gamma point will also speed up the calculations by as much as a factor of 2, because in this k-point, all the Kohn-Sham orbitals can be chosen to be real instead of complex, which reduces the memory requirements and the time spent doing fast Fourier transforms. Large supercells will also need few k-points, because the volume of the Brillouin zone in reciprocal space is very small (due to the inverse relationship). Therefore, only a few k-points (or the gamma point) had to been considered here in the case of the cathode material supercells in Paper II and Paper III.

2.8 Charge-density fitting

DFT in combination with an LCAO basis, formally scales as N^4 (although in practice it can be as good as N^2 with appropriate screening of multi-center two-electron integrals). Yet in a periodic approach, with a plane wave basis, the formal scaling is N^3, limited by the diagonalization of the Hamiltonian, because the fast Fourier transform part of the calculation scales as $N \log N$. This implies that it should be possible to improve upon the standard LCAO method. The way of accomplishing this is called charge-density fitting, or sometimes the resolution-of-identity approximation, where an auxiliary basis-set is used to decompose the electron density[49]. It reduces the computation of four-center two-electron integrals into a product of two three-center integrals, whereby the scaling is formally reduced to N^3. In practice, speed-ups of a factor ten is not unusual. The resolution-of-identiy approach was used in all

Turbomole calculations with the built-in charge density fitting basis[2]. The error introduced is typically small (<0.3 kJ/mol [49]) but can be greater in some cases, such as transition metals with certain electron core potentials [50].

2.9 Numerical grids

The exchange-correlation in DFT is usually calculated by numerical integration over a grid (although it is technically possible to calculate it using a basis set for high-precision calculations). In VASP, the density of the grid is controlled by the FFT mesh points that are used to do the calculation in reciprocal space. Normally, the FFT grid point density is determined as function of the plane-wave energy cut-off, so convergence of the exchange-correlation energy is automatically done in conjunction with the normal basis set convergence tests.

In TURBOMOLE, a multigrid approach is used; the multigrids are built up with a radial Gauss-Chebyshev grid [51] and Lebedev angular grids. A quick check of the integration grid precision can be done by comparing the number of numerically integrated electrons to the actual integral number. Doubtful cases can then be checked using an energy convergence test. The TURBOMOLE multigrid (`m4`) was found sufficient in the cases considered here (electronic density accurate to a relative precision of at least 10^{-3}).

2.10 Geometry optimizations

In all papers, geometry optimizations have been performed in order to "relax" an initial crystal or molecule into a stable geometry. This is done by exploring the Born-Oppenheimer potential energy surface using various nonlinear optimization methods. A successful optimization will locate a stationary point on the surface, but one cannot be sure if this is the global energy minimum, because the standard methods only locate the stationary point closest to the geometry from which they start, which might be a local minimum, or even a saddle point. The most complicated cases in this thesis were the SWNT-cluster complexes. Some of the optimization runs required close to 1000 relaxation steps, and exploration of several starting geometries. They also suffered from a wide spectrum of eigenvalues in the Hessian matrix, which slowed down the relaxations due to the high numerical accuracy needed to get rid of noise in the calculated forces.

In the studies performed with VASP, the approach to geometry optimization depends on the size of the simulation cell. For smaller cells, it is beneficial to use a two-step process where one, or several, conjugate gradient (CG) optimizations are followed by a Quasi-Newton scheme with direct inversion of

[2]Called `Ahlrichs Coulomb Fitting` in the EMSL basis set exchange, `https://bse.pnl.gov/bse/portal`

iterative subspace (QN/DIIS). The CG algorithm is more robust and suitable for initial optimization of a cell structure originating from experimental measurements, whereas the QN/DIIS algorithm is very efficient near a stationary point. For larger cells (>50 atoms) with many degrees of freedoms, a damped molecular dynamics algorithm was found to be more efficient then CG, once a suitable combination of parameters (time step and damping factor) had been found. The damped molecular dynamics method is effectively a primitive way of doing simulated annealing.

In TURBOMOLE, the `relax` program module with default parameters was used to optimize structures. It employs a combination of schemes, starting with intra/extrapolation of earlier structures, if available, and then proceeds with a QN/DIIS algorithm, similar to VASP. Redundant internal coordinates[52] were generated for the cluster complexes to speed up the relaxation. Some tricky cases were partially relaxed in Cartesian coordinates.

3. Summary of the papers

This chapter presents the most important results of the papers included in the thesis, discussed in the context of other papers presented here, and in the literature. Some implicit points in the papers are also presented here.

Paper I (The Li_2FeSiO_4 cathode material)

In paper I, a density functional theory study was made on lithium iron silicate (Li_2FeSiO_4)[53], both fully lithiated, having two lithium ions per formula unit, and partially lithiated having one lithium per formula unit. Lithium iron silicate is an emerging alternative to cathode materials for upscaled Li-ion battery applications, owing to its potentially lower cost and better safety properties[54].

The background was to confirm the experimental crystal structure in ref. [53], which was challenging to determine by X-ray diffraction (XRD), and to gain insight into electrochemical properties such as the necessary voltage to extract more than one Li ion per formula unit (f.u.). The partially lithiated state allows for many permutations of the Li ionic positions and was therefore investigated in three different configurations (see Fig 3.1). The first finding was that the calculated intercalation voltages for Li_2FeSiO_4/$LiFeSiO_4$ (2.7-2.9 V) were not as bad as one might expect due to the kind of material involved, which often exhibits strong correlations; the error is ca. 10% (vs. 2.8-3.1 V experimentally). The voltage for complete extraction of 2 Li/f.u. from Li_2FeSiO_4 was very high ($\sim$5 V), however, indicating that it would not be possible to realize experimentally. It was further found that different configurations of Li_1FeSiO_4 differ substantially in energy, indicating that only one configuration is likely to be present at normal conditions. This is important because it implies that diffusion of Li ions in the 50% delithiated state will be poor, since the ions would need to jump from one site to another, thus transitioning into a different (local) configuration. It also suggests that several metastable phases may exist, which is one way to explain the experimental drop in voltage seen after the first charge cycle. A finding of this study that was not highlighted specifically in the paper is that the DFT relaxed structure changed into corner-sharing LiO_4- and FeO_4 tetrahedrons instead of edge-sharing (see Fig. 3.2), thus confirming the suspicion that the experimental fitting of the crystal structure was not optimal. Recently, a Japanese group [55] proposed an alternative structure featuring twisted SiO_4-FeO_4 chains. The same structure was later refined from XRD data from Li_2FeSiO_4 nanoparticles in ref. [56].

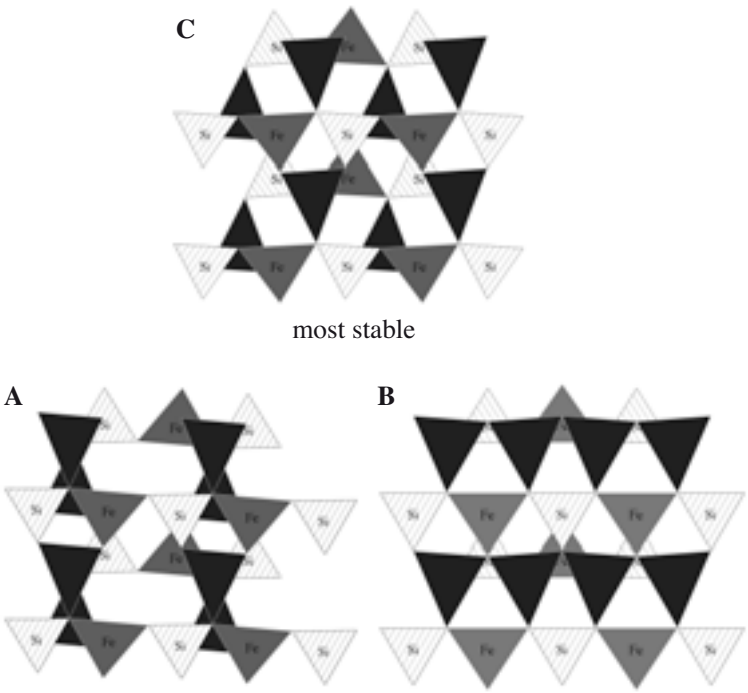

Figure 3.1: The three different crystal structures (A,B,C) of $LiFeSiO_4$ considered in the Paper I, here expanded as 2x2x1 supercells for ease of visualization. Note the position of the solid black tetrahedra (▲) representing Li ions coordinated with oxygen atoms, binding the FeO_4-SiO_4 layers together. Structure C is considerably more stable than the others.

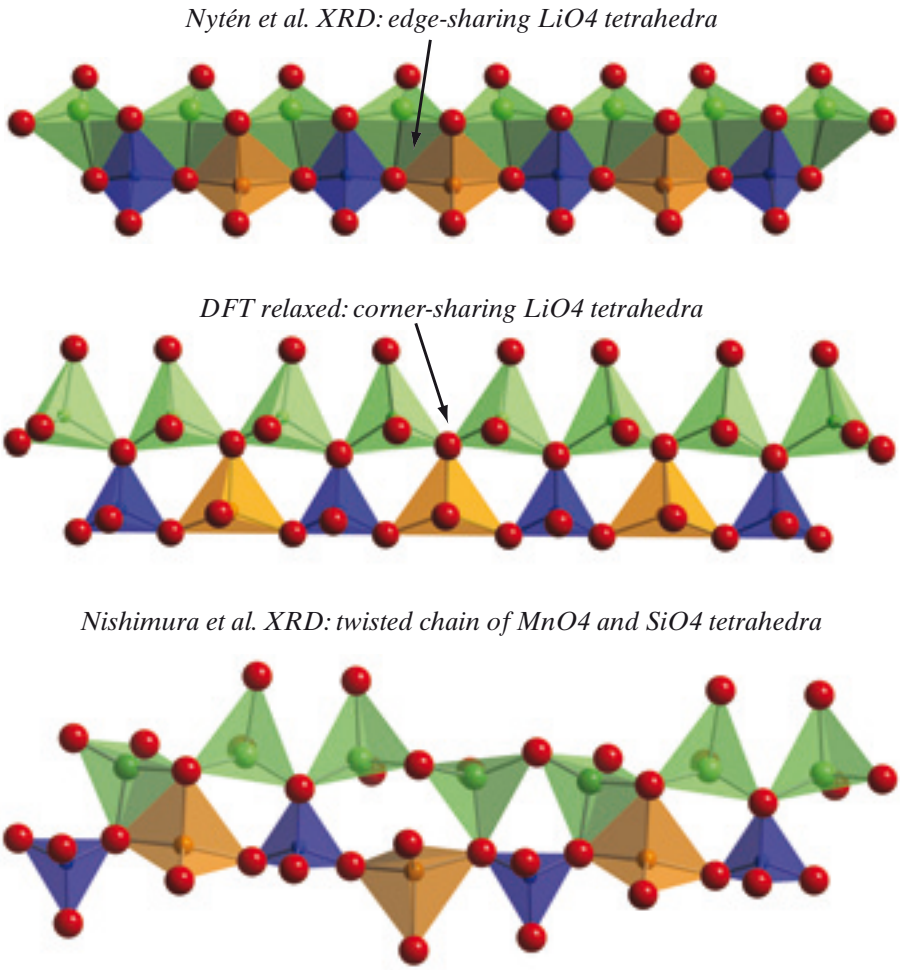

Figure 3.2: Different Li_2FeSiO_4 structures. Top: XRD from Nytén et al. Middle: DFT relaxed structure from Paper I. Bottom: New XRD structure by Nishimura et al. [55]

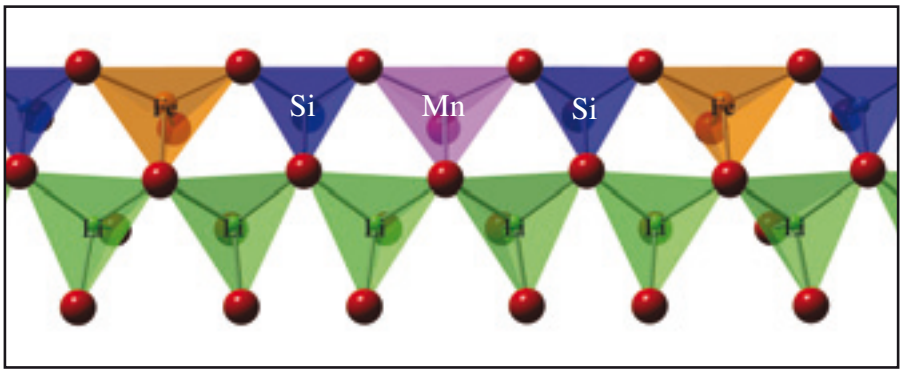

Figure 3.3: Idealized crystal structure of Li_2FeSiO_4 doped with Mn in Fe-sites. Such a material could potentially release more than 1 Li ion per formula unit due to the higher oxidation states of Mn.

Paper II (The $Li_2Fe_{0.875}Mn_{0.125}SiO_4$ cathode material)

One obvious way to engineer the Li_2FeSiO_4 material into higher performance would be to substitute Fe for Mn (see Fig 3.3); Mn can often reach higher oxidation states, e.g. 4+, and thus the capacity of the material could potentially be doubled. Full substitution in the form of Li_2MnSiO_4 has been attempted, but not without loss of reversibility – meaning that the cathode cannot be electrochemically cycled[57]. Presumably, this is due to structural collapse and spontaneous phase separation into amorphous phases upon delithiatation [58, 59]. Here, a study of *partial* substitution of Fe was performed (together with unpublished experimental work) to try to ascertain if the partially substituted material is more stable. Special emphasizes was paid to signs of structural changes and change in electrochemistry.

The crystal structure of Li_2FeSiO_4 from Paper I was used as starting point for the fully lithiated 12.5% Mn-substituted $Li_2Fe_{0.875}Mn_{0.125}SiO_4$ system, and for several delithiated compositions of $Li_xFe_{0.875}Mn_{0.125}SiO_4$, with x in the range 2.0-0.875. In order to achieve a 12.5% concentration of Mn ions, a 2x2x1 supercell containing 64 atoms had to be generated; this allowed one out of the eight Fe atoms in the supercell to be replaced by Mn. Most of the calculations in the paper were done before the monoclinic $P2_1$ structure for Li_2FeSiO_4 was published[55], so we were not aware of it, but it should be noted that the energy difference between these two closely similar structures is < 7 meV/f.u. [Unpublished results]. Also, in the literature, DFT calculations of Li_2MSiO_4 (M=Mn, Fe) in the space group $Pmn2_1$ are available for direct comparison.

From a crystal structure point of view, the main finding was that the structure is surprisingly stable with respect to cell parameter changes when one Fe is replaced by Mn, even when more than 1 Li/f.u. is extracted from the structure (see Table 3.1 and 3.2). There were indications, however, of a distortion of O-Mn-O angle. This is bad news for achieving a higher performance material, since it would impair reversibility.

Table 3.1: *Calculated changes in cell parameters with respect to the fully lithiated $Li_2Fe_{0.875}Mn_{0.125}SiO_4$ structure for the delithiated $Li_xFe_{0.875}Mn_{0.125}SiO_4$ structure for x=1.0 and arrangements (1), (2) and (3) for x=0.875. Experimental values for $LiFeSiO_4$ are given for comparison[60].*

Structure	Method	$\Delta a/a$ (%)	$\Delta b/b$ (%)	$\Delta c/c$ (%)	$\Delta V/V$ (%)
$LiFeSiO_4$	Expt.	3.8	-2.1	-0.3	1.4
$Li_8Fe_7MnSi_8O_{32}$	GGA+U	-3.6	4.0	1.1	1.3
$Li_7Fe_7MnSi_8O_{32}$ (1)	GGA+U	-3.6	4.3	0.9	1.4
$Li_7Fe_7MnSi_8O_{32}$ (2)	GGA+U	-3.6	4.6	0.9	1.6
$Li_7Fe_7MnSi_8O_{32}$ (3)	GGA+U	-3.7	4.3	0.7	1.1

Table 3.2: *Averages of bond lengths and the bond angle within the MnO_4 and FeO_4 tetrahedra for varying x in $Li_xFe_{0.875}Mn_{0.125}SiO_4$; the different configurations are shown as superscripts; standard deviations in brackets.*

x	Fe-O/Å	Mn-O/Å	O-Fe-O/deg	O-Mn-O/deg
2.0	2.044(31)	2.090(12)	127.2(4)	124.2
1.125	1.905(23)	2.084(55)	122.1(2.4)	117.6
1.0	1.903(15)	1.919(27)	122.3(1.0)	135.6
0.875^1	1.901 (23)	1.888(46)	122.7(2.2)	140.6
0.875^2	1.903(22)	1.837(35)	123.1(2.1)	135.3
0.875^3	1.902(22)	1.833(37)	122.9(1.9)	138.0

Table 3.3: *DFT intercalation voltages for $Li_2Fe_{0.875}Mn_{0.125}SiO_4$ vs. Li/Li^+ when removing 1 and 1.125 Li-ion per formula unit. For $Li_{0.875}Fe_{0.875}Mn_{0.125}SiO_4$, three different configurations are shown. In all cases, the voltages are too high for practical use.*

Structure	Voltage vs. Li/Li^+
$Li_8Fe_7MnSi_8O_{32}$ (C)	3.33
$Li_7Fe_7MnSi_8O_{32}$ (1)	4.82
$Li_7Fe_7MnSi_8O_{32}$ (2)	4.86
$Li_7Fe_7MnSi_8O_{32}$ (3)	4.70

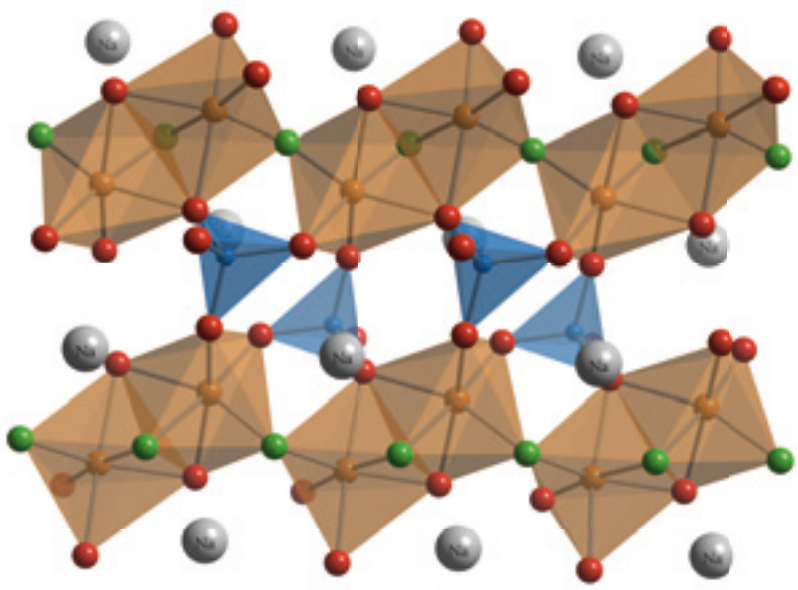

Figure 3.4: Crystal structure of Na_2FePO_4F. Bioctahedral $Fe_2O_7F_2$ units are shown in orange. PO_4 tetrahedral are shown in blue. They form a framework that intercalate lithium and sodium ions reversibly. Sodium atoms are shown in gray color and are labeled "Na".

Electrochemically, the DFT calculations of intercalcation voltages (see Table 3.3) unfortunately indicates that extraction of >1 Li per f.u. from the system still cannot happen except at very high potentials (4.7-4.8 V). These voltages are too high to be able to be used with standard electrolyte systems. It thus appears that not even a low amount of doping of Mn into Fe-sites (12.5%) is capable of enhancing the capacity of Li_2FeSiO_4 in a practically useful way beyond that attainable for the unsubstituted material. The fundamental reason is that the MnO_4 subunits and the Mn^{3+}/Mn^{4+} oxidation reaction is not affected much by interaction with the rest of the crystal lattice and retain the same chemical properties as in the more highly doped materials.

Paper III (The Na_2FePO_4F cathode material)

In paper III, an initial study of the electronic structure of the recently discovered cathode material lithium/sodium iron flourophosphate[61], is presented. This material has the special ability of being able to intercalate sodium, opening up the possibility of making a sodium-ion cell, which is attractive from a cost perspective. The reversible capacity was also reported to be relatively good, ca. 0.8 Na/f.u. out of a total of 2 Na/f.u. could be extracted.

The DFT studies started by setting up the experimentally determined crystal structures (see fig 3.4) and doing geometry relaxations. It was assumed that

the structure of Li_2FePO_4F was similar to Na_2FePO_4F, so the same atomic positions was used, but with the appropriate cell parameters. The procedure was carried out with different functionals, and the +U correction, in order to establish their relative accuracy. It was suspected that these kinds of materials would benefit from an LDA+U or GGA+U treatment due to the similarity with other cathode materials like $LiFePO_4$ and Li_2FeSiO_4.

The PBE and PBE+U results are presented in Table 3.4. The cell parameters are reproduced with reasonable accuracy (5% too small volume/overbinding) with PBE and by using a U value of 4 eV, the agreement is improved a little bit, but the Hubbard correction alone is not enough to reproduce the experimental cell parameters. It would be interesting to further study the origin of this error, since the PBE performs very well for e.g. Li_2FeSiO_4, where the volume error compared to experiment is only 1%.

Table 3.4: *DFT structural parameters for Na_2FePO_4F and Li_2FePO_4F and their delithiated forms. As expected, PBE+U improves cell parameters compared to a pure PBE treatment.*

Compound	Method	a (Å)	b (Å)	c (Å)	Cell Volume (Å^3)
Na_2FePO_4F	PBE	5.11	13.72	11.68	820
	PBE+U	5.13	13.73	11.73	827
	Expt.[61]	5.24	13.87	11.80	858
Na_1FePO_4F	PBE	5.03	13.83	11.36	790
	PBE+U	5.04	13.83	11.31	788
	Expt.[61]	5.10	14.13	11.37	820
Li_2FePO_4F	PBE	4.95	12.96	11.17	717
	PBE+U	4.95	13.09	11.17	724
	Expt.[61]	5.05	13.56	11.05	758
Li_1FePO_4F	PBE	4.98	13.05	11.08	721
	PBE+U	4.99	13.05	11.05	720
	Expt.	n/a			

Delithiated structures were constructed from the fully lithiated structures by removing Na and Li ions from the least stable group of sites (the structures have two sets of equivalents sites), and then geometry optimized. The structure for Li_1FePO_4F has not yet been determined experimentally, but the resulting geometry for Na_1FePO_4F are just as before, close to the experimental one, but with a little bit too small volume, the error is ca. -4%. In this case, adding the Hubbard correction changes the resulting cell parameters and volume very little.

With knowledge of the total energy for both the full lithiated and delithatied phases, ab initio intercalation voltages could be determined. While the Hubbard correction improved structural constants somewhat, it would be expected

to be more critical here. This was also what was found. The results are shown in Table 3.5. The voltages are far too low when calculated with PBE, but PBE+U (with U = 4.0 eV) recovers about half of the missing potential differences. It is highly interesting that the LDA+U do give voltages very to the experimental ones. It suggests that one may use GGA to relax the structures, and then determine intercalation voltages, and perhaps other properties, by LDA+U single point calculations. (This is similar to what some people do when studying magnetism: optimize structures with GGA and determine magnetic moments afterwards with LDA.)

Table 3.5: *Calculated intercalation voltages of cathodes based on the Na_2FePO_4F / Na_1FePO_4F and Li_2FePO_4F / Li_1FePO_4F reactions vs sodium and lithium metal.*

Redox couple	Method	Voltage vs Na (V)
Na_2FePO_4F / Na_1FePO_4F	PBE	2.64
	PBE+U	3.04
	LDA+U	3.19
	Expt.[61]	3.50
Li_2FePO_4F / Li_1FePO_4F	PBE	2.98
	PBE+U	3.38
	LDA+U	3.54
	Expt.[61]	3.50

Paper IV (Carbon nanotubes + metal rings)

Some preparatory results regarding methodology of how to calculate binding strengths of metal catalysts to carbon nanotubes (related to Paper V) are presented here. It is investigated what metal structures that can be used to model carbon nanotube-metal surface interactions. There had been earlier studies on single atom interactions with the ends of nanotubes, but there was reason to believe that a single atom was not enough to describe the interaction with a metal surface, which has much more energy dispersion.

In general, one always wants to use the smallest possible model that can capture the relevant properties. It is mainly due to the computational expense involved with larger systems, but it also helps to analyze and isolate effects. So what is the smallest model that could possibly work? The smallest SWNTs that has been observed are the (3,3) and the (5,0), with diameters of about 4 Å, see Fig. 3.5. Anything smaller appears to be too strained. The (5,0) tube was chosen as the minimal system mainly due to its high rotational symmetry (C_{5v} group), which speeds up calculations with Gaussian basis sets in non-periodic settings (although not explicitly used here, since the complexes were

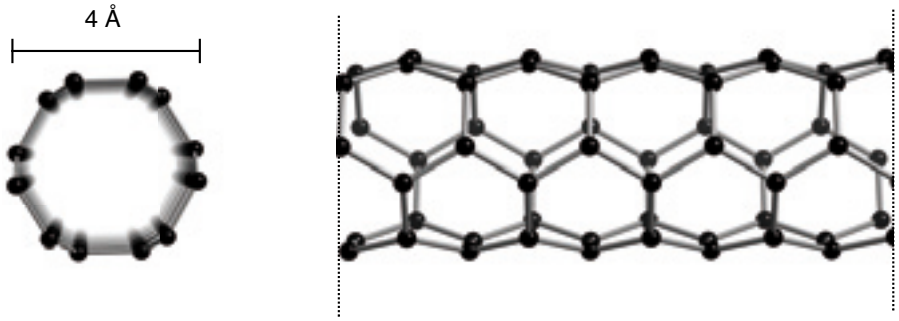

Figure 3.5: Picture of a (3,3) nanotube–one of the smallest diameter nanotubes that have been observed experimentally.

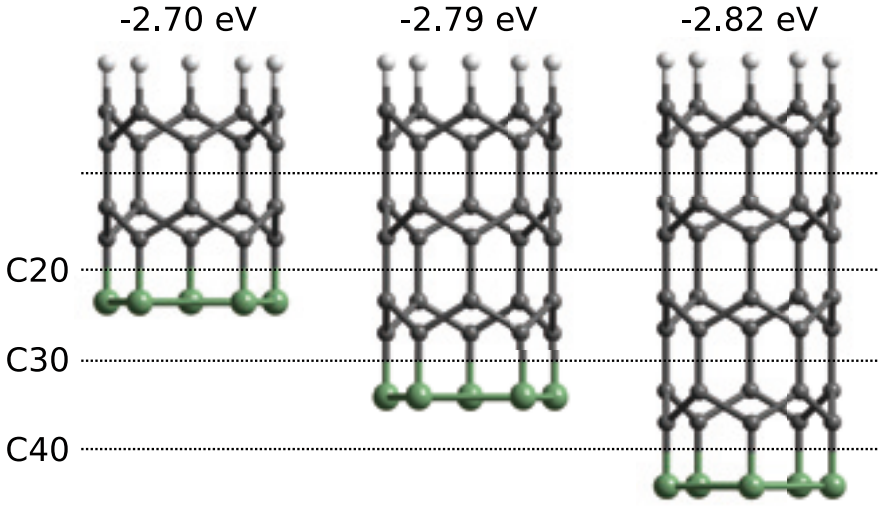

Figure 3.6: Pictures of (5,0) tubes of different lengths attached to rings of metal atoms in the end. The total binding energy appears to be converged to < 0.1 eV when using three SWNT unit cells.

calculated in supercells with VASP and C_5-symmetry is not supported in the crystallographic space groups).

The influence of SWNT length was studied for a (5,0) tube using the structures shown in Figure 3.6. The adhesion energy of a 5-atom Ni-ring is not very sensitive to the length of the nanotube. Even the minimal configuration of two unit cells in the axial direction of the nanotube captures 95% of the interaction energy (-2.70 eV/atom) obtained with four unit cells (-2.82 eV/atom). The reason that the binding energy is larger for the longer tube (one would otherwise expect that shorter tubes are more unstable and therefore bind stronger to a metal atom) is likely related to delocalization effects: any induced polarization of the electron density due to binding will be easier to incorporate in a larger tube fragment.

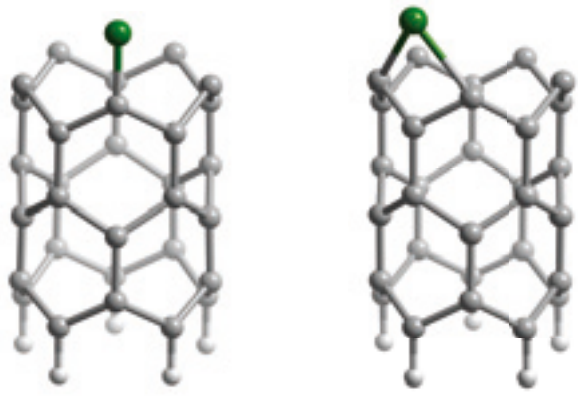

Figure 3.7: Pictures of a (5,0) tube with a single metal atom at the end; two positions, *top* and *middle* are shown.

The most simple approach to measuring the SWNT-catalyst interaction strength is to use a single metal atom and attach it to the nanotube. The two extreme positions of a single metal atom bound to an SWNT end is shown in Figure 3.7. A single metal atom will, as expected, be most stable in a position in between two carbon atoms at the end of the tube (*middle* position). This way, it can interact with two carbon atoms. The binding energy is 5.5, 5.2 and 4.6 eV for Fe, Co and Ni, respectively; one may keep in mind the order Fe $>$ Co $>$ Ni. It is possible to calculate the binding energy of the "top" position, but this arrangement is not stable with respect to geometry optimization.

The next step in complexity is to model the metal interface as a ring of atoms bonded to the SWNT end, shown in Fig. 3.8. In this case, the lowest energy structure is different from the single atom case–it is a ring with metal atoms aligned in the *top* position. This outcome holds for Fe, Co, Ni and is also independent of geometry optimization. It suggests that the chemical interactions are fundamentally different when metallic systems interact with the SWNT end, as compared to isolated metal atoms (e.g. in gas phase). The stability of the top position can be understood from the point of view of the SWNT end: placing a metal atom directly above a carbon end allows a natural continuation of the graphene sheet's sp^2-type bonding. The bond between the metal atoms will also be less covalent, and more metallic. Since this is an effect that depends on the configurations of at least 3 atoms, one can also draw the conclusion that pair potentials cannot accurately describe the metal-SWNT interface.

The binding energies for the rings are 3.4, 3.2, and 2.9 eV for Fe, Co, Ni, respectively. It means that the trend in binding energies of Fe, Co, Ni is still the same as predicted from the single atom calculations, but the binding strength values are not.

A step further is to consider a larger body of metal atoms interacting with the SWNT end. A large cluster will have a very small band gap and behave

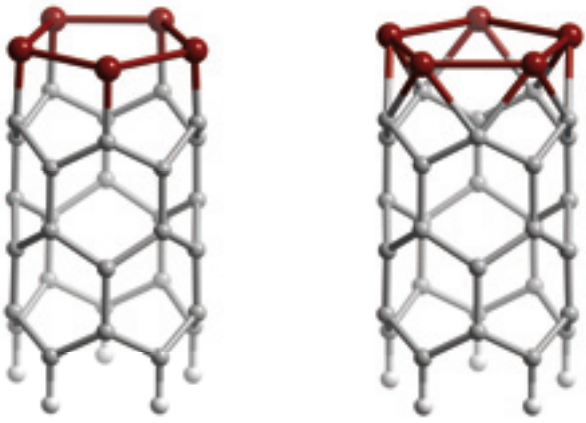

Figure 3.8: Pictures of a (5,0) tube with a ring of metal atoms at the end; two positions, *top* and *middle* are shown.

similarly to a bulk metal. If modeling the metal interface as a ring gave different results compared to single atom, perhaps an even larger body of metal atoms will change the outcome? The M_{13} cluster with icosahedral symmetry is a good choice to pair with the (5,0) SWNT. It is five-fold symmetric, so that it matches the SWNT end, and the cluster geometry is also a global energy minimum ("magic number") for Fe, Co, Ni. Similar to the metal rings, one can attach the cluster with metal atoms aligned in *top* or *middle* positions, see Fig. 3.9.

It turns out, however, that the difference with cluster models is very small. The essential chemical properties seem already to be converged with the ring model. A chart of the binding energies (see Figure 3.10) in the most stable positions shows that the difference between Fe, Co and Ni grows smaller as the number of metal atoms increases, and the system becomes more metallic. Also the trend in binding energies is roughly the same.

Paper V (Carbon nanotubes + metal clusters)

A study of the literature of carbon nanotube growth reveals that certain metals are used exclusively when growing nanotubes using carbon vapor deposition (CVD), laser ablation and arc discharge method. Why is that so? In the case of CVD, the traditional explanation is that the catalyst particles must have properties such as being able to split the carbon feedstock gas and dissolve the splitted carbon. In this paper, another criterion is highlighted: that the catalyst particle-SWNT adhesion needs to be sufficiently strong. It must be so in order to stabilize the hollow graphitic structure that grows into a nanotube and prevent it from losing connection to the catalyst particle. It is found that this sufficient strength is a property of the popular Fe/Co/Ni-based catalysts. One

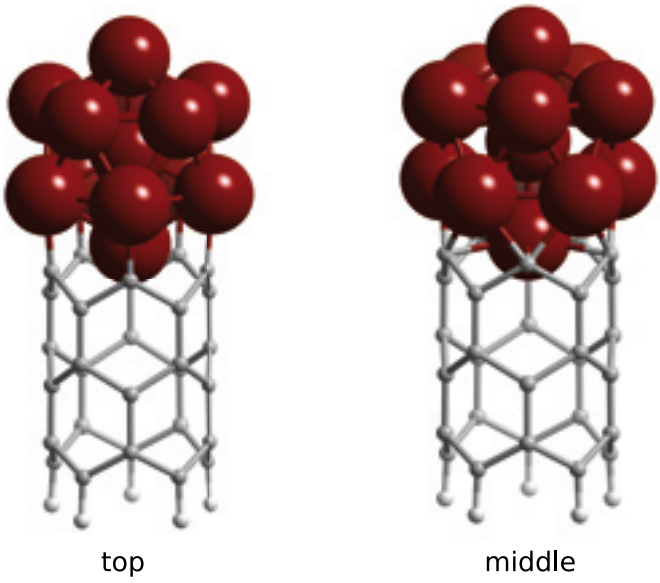

Figure 3.9: Pictures of a (5,0) tube connected to 13-atom icosahedral clusters; two positions, *top* and *middle* are shown.

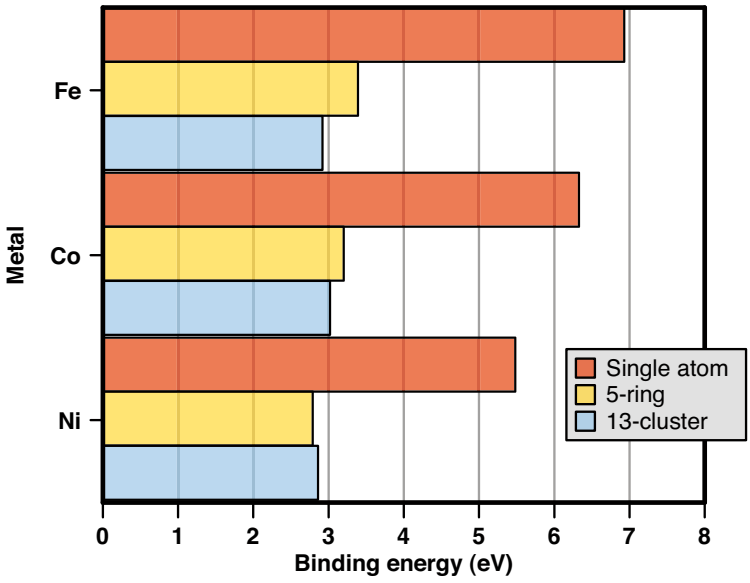

Figure 3.10: Metal binding energies to (5,0) SWNT ends using different metal surface models.

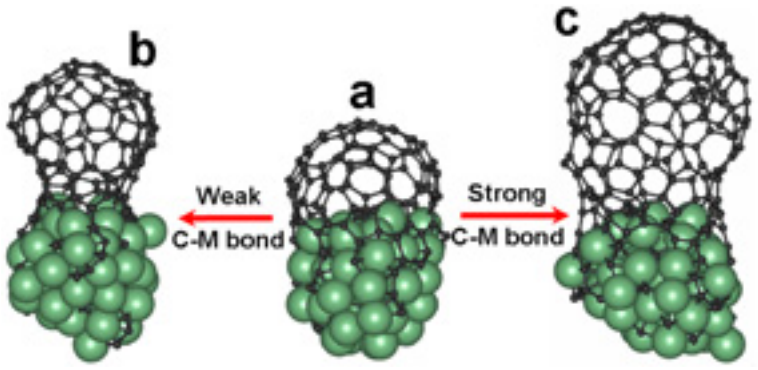

Figure 3.11: Snapshots from molecular dynamics simulations of carbon structure growth on an Fe_{50} nanoparticle. **a**: carbon caps form spontaneously. **b**: too weak carbon-metal bonds lead to fullerene formation. **c**: stronger carbon-metal bonds allow the tube to continue growing.

can note that DFT calculations are especially pertinent here, because determining individual metal-SWNT adhesion strengths experimentally would be extremely challenging. It would, for example, require pure samples of nanotubes with a certain chirality and atomic level control. Therefore, this study is a good choice for ab initio calculations.

The hypothesis of sufficient adhesion strength came from observations in semi-empirical MD-simulations of the growth of carbon nanotubes. In these simulations, Fe_{50} particles were fed carbon atoms (by continuously putting C atoms on the surface of the cluster), and carbon structures could be seen forming on the surface of the particle (see Fig. 3.11a). The striking effect was that the morphology of the carbon structures seemed to depend on the metal-carbon bond strength used in the simulations. If the carbon-metal bonds were weaker than the carbon-carbon bonds, the tube end lost connection to the metal surface and fullerene structures formed (Fig. 3.11b), while if the metal-bonds were stronger, growth continued (Fig. 3.11c). The idea was that commonly used metal catalysts would display the same strength of carbon-metal bonds with respect to carbon-carbon bonds. The bond strengths were artificially controlled with a parametric force field, however, so it remained to determine the actual bond strengths of the different metals.

In paper IV, the minimal model characteristics were investigated, and a ring + metal end model was found to be the smallest acceptable. Here, M_{13} and M_{55} cluster models were used, mainly to be on a safe side, but also because the bigger systems turned out to be feasible to run as larger computer resources became available. The ring model also showed a slight tendency to exaggerate the difference between metals, and since one of the aims were to compare different metals in order to look for signs of e.g. chirality selection, it would be advantageous to minimize spurious differences.

In order to capture chirality effects, two sets of SWNTs were used, zigzag (5,0) and (10,0) and armchair (3,3) and (5,5). As noted before, the smaller

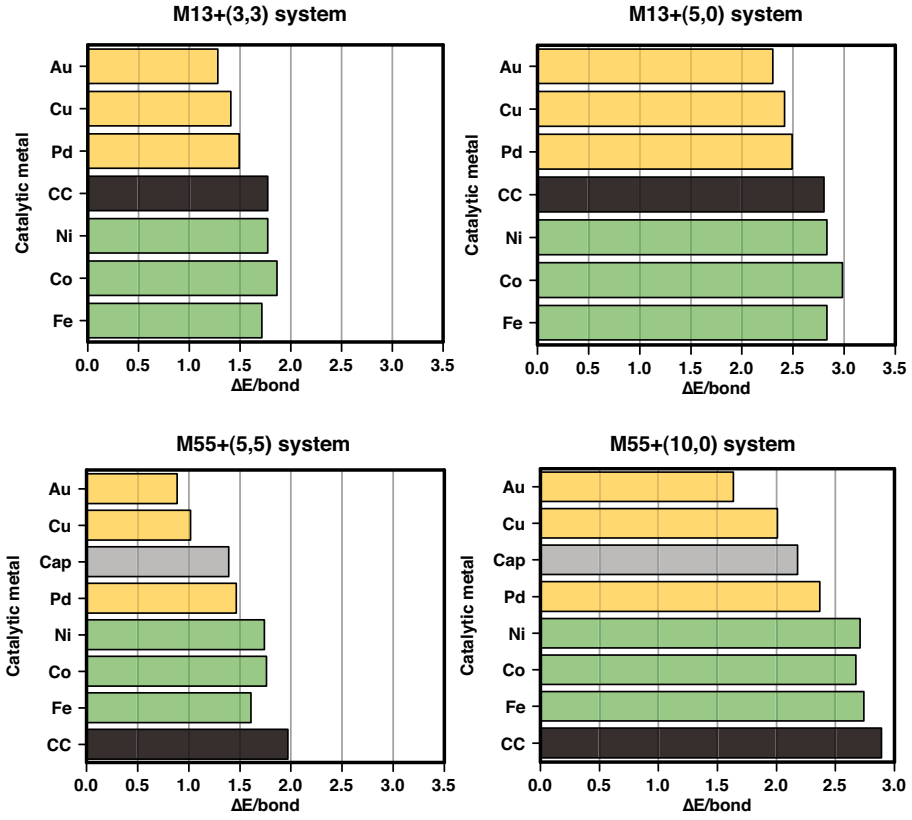

Figure 3.12: Calculated binding energies of 4 different metal nanoparticle + SWNT systems, compared with carbon-carbon bond strengths calculated from the dangling bond ("CC") and cap formation ("Cap") energies.

tubes are not naturally stable so one can expect the binding energies to the metal surface to be somewhat overestimated for the (3,3) and (5,0) nanotubes. Magnetic effects will also be enhanced for the smaller clusters and introduce some noise when comparing bond strengths.

The calculated binding energies when carbons are attached in *top* positions are shown in Fig. 3.12, together with two reference binding energies: C-C (dangling bonds) refer to the energy required to cut a nanotube fragment into two pieces (of the same size as the one used to calculate binding energy to metal clusters); C-C (cap formation) is the energy gained when the open-ended nanotube fragments forms a capped end with fullerene geometry. It can be seen that iron-like metals (Fe, Co, Ni) always come out higher than the coinage-type metals (Au/Cu/Pd). This finding, together with the preference in experiments to use iron-like metals, confirms the hypothesis laid out earlier, viz. that strong metal-carbon interactions are important for continued growth and that only certain metals display that property.

Similar findings were recently published by Yazyev and Pasquarello [62], who calculated the binding strengths of carbon atoms and benzene fragments

to metal surfaces. They expressed their results as chemical potentials, obtaining the order

$$\mu(\mathrm{Ni}) < \mu(\mathrm{Pt}) < \mu(\mathrm{Pd}) < \mu(\mathrm{Cu}) < \mu(\mathrm{Au}) < \mu(\mathrm{Ag}), \tag{3.1}$$

which agrees with the calculations presented here.

One might ask what is the critical value of the carbon-metal bond? To answer this question one must specify a necessary criterion for continued nanotube growth. A natural criterion arises from the MD observations of fullerene formation and closure of the tube end: if the energy gained from closing the tube end and forming a cap is greater than the binding energy, dissociation will occur spontaneously (in the thermodynamical sense). The tube closure reaction would be:

$$\mathrm{M_{55}SWNT} \rightarrow \mathrm{M_{55}} + \mathrm{SWNT(open-ended)} \rightarrow \mathrm{M_{55}} + \mathrm{SWNT(capped)}. \tag{3.2}$$

(Note that the smaller tubes have no stable caps, so only the larger tubes can be used for this calculation.) The reaction energies for the (5,5) and the (10,0) tubes are shown in Fig. 3.13. They highlight relative binding strengths of different metals with respect to the energy gained by the SWNT dissociating and forming a cap. One sees that Au and Cu cannot maintain an open tube end connected to their metal surfaces under equilibrium conditions, i.e. energy would be gained by closing the tube end, while the iron-like metals, on the other hand, establish bonds that require more than 0.2 eV/bond to break, making them stable even at high temperatures (for comparison, 1 kT at 900 K is 0.077 eV).

It is possible to define another criterion for nanotube growth. The reaction energies derived from Eq. 3.2 are only valid in equilibrium conditions. Out of equilibrium, it might be more useful to consider the activation energy of dissociation–corresponding to the first step in Eq. 3.2. Still, it is a catalyzed process, so the binding energies used here as a proxy for the activation energy should be seen as the upper bound, since the actual barrier is expected to be much lower. In this picture, all metal-SWNT complexes with a sufficiently high activation energy of dissociation should be able to grow nanotubes in out-of-equilibrium conditions. In fact, the first successful attempts of growth of SWNT on Au nanoparticles were recently reported[63, 64].

It is interesting to analyze the cap formation criterion in terms of chirality. Are there metals which would preferably grow tubes of a certain chirality? We find some indications of it being possible. In Fig 3.13, one can look at the difference between (10,0) and (5,5) reaction energies. For some metals, like Fe and Cu, it is rather large. Therefore, it might be possible that there exists alloys that display negative ΔE for one particular chirality, but positive ΔE for others, or the other way around. In that case, those alloys would display chiral selectivity and grow a high proportion of one kind of nanotubes. Consider, for example, a hypothetical $\mathrm{Fe_{0.50}Cu_{0.50}}$ alloy derived from the results in Fig 3.13. The ΔE would, by linear combination, become -0.8 eV for (5,5) SWNTs and 1.9 eV for (10,0) SWNTs, shifting the yield towards zigzag-type SWNTs.

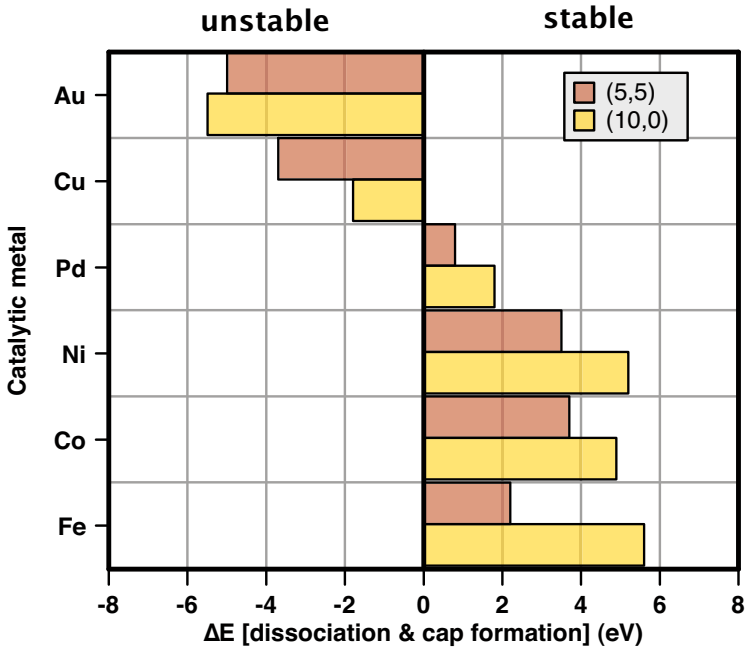

Figure 3.13: Tube dissociation and closure reaction energies. The negative energies obtained for Au and Cu particles imply that they cannot keep the growing end of the SWNT open.

Paper VI (Growing carbon nanotubes on Cu/Mo particles)

In this paper, the predictions of paper V are put to the test experimentally by trying to grow carbon nanotubes using copper/molybdenum nanoparticles. Copper is traditionally believed not to be able to catalyze nanotube formation, although it can catalyze carbon fiber formation (see e.g. the review by Baker[65]). Recently, though, there have been surprising reports about successful growth on Cu particles[63]. Molybdenum, on the other hand, is a known catalyst additive, known to improve carbon nanotubes yields. But molybdenum cannot grow nanotubes by itself, because at temperatures > 700 °C, the very stable compound molybdenum carbide forms. The question is what happens when these two catalytic metals combine. According to the hypothesis laid out in Paper V, the carbon nanotube binding strength of Cu+Mo, supposedly falls in between that of it alloying components, and may be expected to be similar in strength to catalysts such as Fe, Ni and Co, and therefore able to stablize a growing CNT end.

No DFT calculations for Mo were presented in Paper V, so it was necessary to do some additional calculations for pure Mo particles, and Cu/Mo mixtures in order to prove that the catalyst-SWNT binding strength indeeed is in the optimal range. As a compromise between the more qualitative ring model used in paper IV, and the full M_{55} clusters used in paper V, a M_{13}+$C_{30}H_5$ system

was used to study the binding of Cu/Mo particles to SWNTs. The different cluster structures considered are shown in Fig. 3.14, and the corresponding SWNTs binding energies in Table 3.6.

The pure Cu_{13} cluster-(5,0) SWNT complex (structure **I**) has a binding energy (per dangling bond or carbon atom at the open end) of 2.29 eV, while the binding energy of the Mo_{13}-(5,0) complex **II** is 3.63 eV. In structure **III**, all of the Cu atoms in the Cu_{13} particle that does not have bonds to the nanotube were replaced by Mo, lowering the binding energy slightly to 2.05 eV. A lower energy (1.73 eV) was also seen in structure **IV**, where the central Cu of structure **I** was replaced by Mo. This effect is however, mostly artificial, since the $MoCu_{12}$ cluster is additionally stabilized by the formation of a closed-shell electronic state, which decreases the calculated binding energy. The results so far, shows that Cu coating of Mo particles gives particles that, compared to pure Cu particles, have the similar, or decreased, ability to stabilize the growing end of a carbon nanotube.

If, on the other hand, the situation is reversed, and Mo is present at the surface of Cu particles (structures **V-VII**) then the binding energy increases, compared to pure Cu, to 2.35 eV for structure **V** and 2.90 eV for structure **VI**. If not only one atom, but the complete surface layer of Cu atoms close to the SWNT, is replaced by Mo (structure **VII**), the binding energy increases as well (2.76 eV), but curiously, not as much as for structure **VI**. The important point, however, is that the latter binding energies are matching the open end carbon dangling bond energy, as was also found for Fe, Ni, and Co in Paper V. Thus, the DFT calculations predict that a composite nanoparticle containing both Cu and Mo should be able to stabilize a CNT growing end.

Table 3.6: *SWNT bindning energies to 13-atom Cu/Mo metal clusters per carbon dangling bond. A pure copper cluster (***I***) does not bind strong enough, but with molybdenum atoms at the surface (***VI,VII***) the binding energy becomes sufficiently strong to compete with the energy gained from closing carbon-carbon dangling bonds.*

Structure	Geometry	Binding energy (eV/bond)
IV	Mo center	1.73
III	Cu top	2.05
I	Only Cu	2.29
V	Mo side	2.35
	C-C dangling bond	2.76
VII	Mo surface	2.76
VI	Mo top	2.90
II	Only Mo	3.63

The experiments were done using CCVD of methane over Cu/Mo catalysts with a MgO support at a temperature of 850 °C. Aside from pure Cu and pure

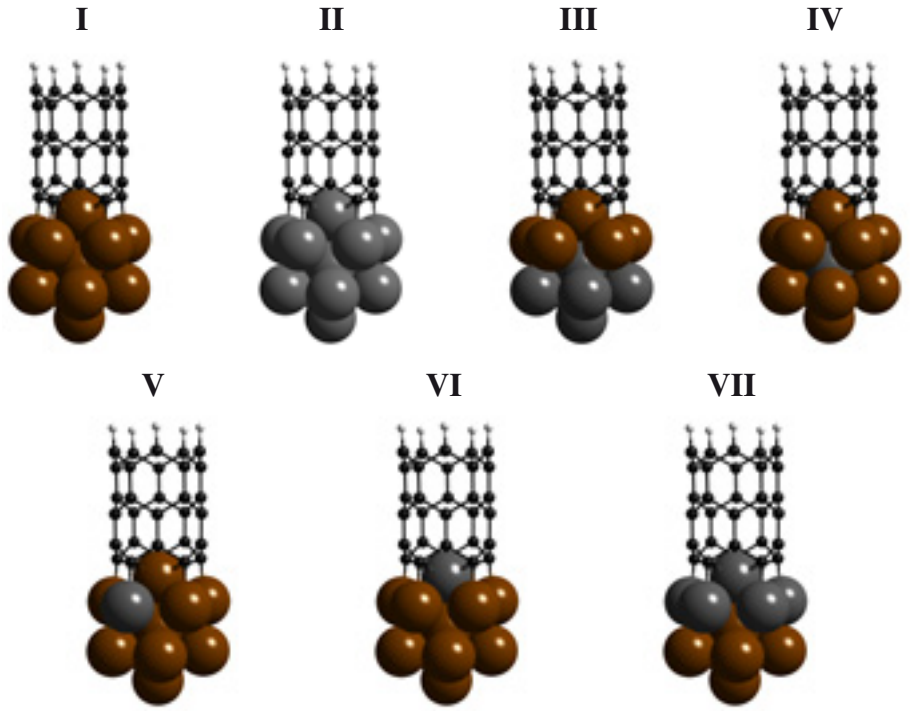

Figure 3.14: The seven different SWNT–cluster complexes used to calculate SWNT–cluster adhesion energies. **I**: Cu_{13}. **II**: Mo_{13}. **III**: Mo_7Cu_6 with copper atoms on the top surface. **IV**: $MoCu_{12}$ with a molybdenum atom in the center of the cluster. **V**: $MoCu_{12}$ with a molybdenum atom directly below a carbon atom. **VI**: $MoCu_{12}$ with amolybdenum atom on top/inside the SWNT. **VII**: Mo_6Cu_7 with molybdenum atoms on the top surface.

Mo, the following catalyst compositions were tried: 1+10, 3+10, 5+10, and 5+2 wt% Mo+Cu (the wt% is compared to the MgO support). Transmission electron microscopy (TEM) and energy dispersive X-ray analysis showed that the observed catalyst nanoparticles were indeed Cu/Mo composites. The outcome of the growth experiments are shown in Table 3.7. In contrast to findings of Takagi and co-workers[63], pure Cu can by itself not catalyze CNT production. Furthermore, no carbon nanotubes could be seen in TEM when using a 10 wt% Cu + 1 wt% Mo catalyst. But with a higher Mo loading of 3 wt%, some yield of nanotubes were obtained, ca 3 wt% with respect to the MgO support. It was not until 5 wt% Mo that significant yield were observed. At this stage, one might be tempted to draw the conclusion that the yield increases with Mo content, and that superior yields may be gotten with a pure Mo catalyst. This is, however, not the case, as is evident from the poor CNT growth observed with 5 wt% Mo and only 2 wt% Cu. There only a few carbon nanotubes could be observed by TEM, and with pure Mo particles, no CNTs were observed at all. This shows that there needs to be an balance of Cu and Mo in order to achieve high-yield growth.

Table 3.7: *Experimental* CNT *yields with different catalyst metal compositions. The compositions are characterized by weight percent compared to the MgO support. Both Cu and Mo need to be present in order to get high yield of carbon nanotubes.*

Mo content	Cu content	CNT Yield
–	5 wt%	0 wt%
–	10 wt%	0 wt%
1 wt%	10 wt%	0 wt%
3 wt%	10 wt%	3 wt%
5 wt%	10 wt%	17 wt%
5 wt%	2 wt%	∼0 wt%
5 wt%	–	0 wt%
10 wt%	–	0 wt%

In summary, by combining the experimental and theoretical results, one can conclude that neither pure Mo nor pure Cu particles can catalyze CNT growth. It is necessary to have both Mo and Cu present in the catalyst in order to produce CNTs. The reasons being, firstly, that Mo is needed to break C-C bonds (i.e. decompose the carbon feedstock gas), and secondly, that only Mo/Cu composite particles have CNT binding strengths in the right range to support CNT growth.

Paper VII (Open-ended carbon nanotubes)

This paper discusses useful mechanisms for increasing chirality selectivity beyond just changing the metal catalysts. It is common to assume that nanotube growth can be controlled thermodynamically by using a growth process that initially favors small tube fragments of certain chiralities. We argue that this will be hard, based on the small energy difference between short tube sections with a given diameter. Consider the DFT total energies for hydrogen-terminated SWNTs with nine, ten, and eleven carbon atoms around the circumference at the end, shown in Table 3.8. The energy difference between two segments with different chirality can be as small as 15 meV. But in a typical CVD process, temperatures can reach 1000 Kelvin, giving a kT of 86 meV. This finding casts doubt on whether a thermodynamical selection of chiralities is at all possible.

Another observation is that the most stable chirality is not the same in different series. Suppose one would like to grow zigzag tubes $(n,0)$ selectively. It could work for the $n+m=9$ and $n+m=10$ series, because (9,0) and (10,0) are the most stable species, but if some $n+m=11$ tubes also formed (due to, for example, not perfectly monodisperse nanoparticles) contaminat-

ing (6,5) tubes would be found, because they are the most stable segments in the $n+m=11$ series.

Table 3.8: *Total energy differences between hydrogen-terminated SWNT segments with similar diameters. The smallest energy difference is of the same order as thermal fluctuations in a CVD experiment.*

Series (n,m)	Max. ΔE (eV)	Min. ΔE (eV)
$n+m=9$	1.38	0.074
$n+m=10$	0.88	0.054
$n+m=11$	0.65	0.015

Table 3.9: *Total energy differences between open-ended SWNT segments with similar diameters. Open-ended SWNTs span an order of magnitude much wider range in energy than closed tube segments.*

Series (n,m)	Max. ΔE (eV)	Min. ΔE (eV)
$n+m=9$	6.87	1.45
$n+m=10$	8.25	1.41
$n+m=11$	8.91	1.57

The findings in paper V suggests, however, that analyzing carbon nanotube formation in terms of a dissociation + cap formation reaction is useful. The activation energy in this reaction is the dissociation step, which depends on the stability of the carbon nanotube open end. The main point of this paper is that utilizing the stability of the tube end offers a more promising route to chirality selection. Too see why, consider the differences in total energies of open-ended SWNT segments constructed by cutting the hydrogen-terminated tube segments into two identical segments according to equation 3.3. By this approach, one can determine the carbon dangling bond formation energy simply by dividing the total reaction energy by the number of carbon dangling bonds present at the interface.

$$\text{H-terminated SWNT} \rightarrow \text{2 open-ended SWNTs} \tag{3.3}$$

Now, in contrast to the H-terminated SWNTs, the total energies of two open-ended SWNTs span the much wider ranges of 13.7 eV, 16.5 eV and 17.8 eV for the $(n+m=9)$, $(n+m=10)$ and $(n+m=11)$ SWNT series, respectively, with considerably larger energy differences (>1 eV) between different chiralities (see Table 3.9). In other words, the open end is much more sensitive to different chiralities. Another change is that the ordering of the open-ended SWNTs

is now the same for all three series, with the most armchair-like nanotubes, viz. (5,4), (5,5) and (6,5), being the most stable and the zigzag nanotubes, viz. (9,0), (10,0) and (11,0), being the least stable. There is an almost incremental increase in energy of 2.9 - 4.5 eV (1.4 - 2.2 eV per half SWNT) for each decrease of the 2nd integer of the nanotube index. It might be possible to exploit this difference in open end stability between armchair and zigzag SWNTs through experimental protocols using selective dissociation of tubes that are more armchair-like than zigzag, since they should have lower barriers of dissociation than zigzag tubes according to Hammond's postulate: the transition state of dissociation of a zigzag tube from a catalytic metal particle should be much higher in energy than the corresponding transition state of an armchair tube because the two product energies differ significantly. One scenario would be adding one, or several, annealing steps after the initial SWNT growth in order to dissociate armchair-like products, followed by continued growth of only the remaining zigzag tubes. If the dissociated armchair tube fragments could be successfully recovered, they may also be regrown separately.

Paper VIII (MgH_2 clusters with transition metals)

Nanocrystalline magnesium powder is a well-studied hydrogen storage material[66, 67], especially when ball-milled with small amounts of transition metal catalyst such as Ti, Nb, V, Fe, Co and Ni. It is well-established that adding transition metals to the nanoparticles greatly enhances the hydrogen release speed, but the underlying mechanism has not been fully investigated. It has been speculated that transition metal hydrides work as "gateways" or "shuttles" for hydrogen, since transition metal hydrides have been observed to remain during the whole dehydrogenation process[68]. In Paper VIII, DFT calculations and geometry optimizations are used to investigate how very small Mg clusters (31-94 atoms) interact with the transition metal atoms Ti, V, Fe, and Ni. One Mg atom out of 31 was substituted, corresponding to ca. 3 mol% transition metal. The motivation was to understand the mechanism of catalysis, rather than bulk alloying. Surprisingly, very few theoretical studies have been done on Mg *clusters* [48, 69, 70], although Mg-alloys are always ball-milled to nanometer size to increase surface area and kinetics.

In order to assess whether this small amount of alloying could destabilize the whole cluster and lower the temperature of hydrogen desorption, reaction energies corresponding to full dehydrogenation for both the pure and transition metal doped MgH_2 cluster were calculated using the following reactions:

$$\Delta E = [E(Mg_{31}) + 31\ E(H_2)] - E(Mg_{31}H_{62}] \tag{3.4}$$

and

$$\Delta E = [E(Mg_{30}M) + 31\ E(H_2)] - E(Mg_{30}MH_{62}] \tag{3.5}$$

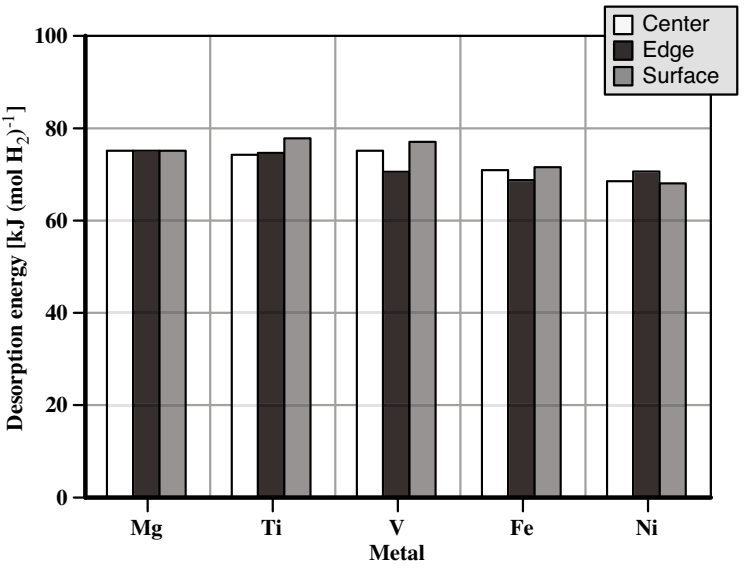

Figure 3.15: Average hydrogen desorption energies for $Mg_{30}MH_{62}$ clusters with three differently positioned dopants, as compared to a undoped $Mg_{31}H_{62}$ cluster. All clusters display roughly the same bulk properties.

These results are shown in 3.15. Reaction enthalpies for all systems lies with a small range of 70 to 80 kJ/mole with the lowest values for Fe and Ni. The doped Mg clusters would all be expected to release hydrogen at temperatures close to the undoped case, as expected for such a low degree of alloying. It is, of course, likely that the effects may be enhanced with a higher amount of alloying, but from a technical point of view, it would lead to lower gravimetric density and thus be undesirable. Mg-transition metal alloys also tend to be inherently unstable.

The reason why the Fe- and Ni-doped clusters have slightly lower reaction enthalpies in 3.15 is surface relaxation effects near the dopant atoms. One may therefore suspect that dehydrogenation energies of hydrogen atoms adjacent to dopants are influenced much more. This effect can be quantified by calculating the removal energies of single hydrogens attached to transition metals using the following formula:

$$\Delta E = Mg_{30}MH_{61} + 0.5\ E(H_2) - E(Mg_{30}MH_{62}). \tag{3.6}$$

The resulting energies (given in Fig. 3.16) highlight the local effects of metal dopants. In MgH_2 nanoclusters, the removal of hydrogen bound to edge site atoms is endothermic, while the process is exothermic for the surface atom. This demonstrates that nanostructuring can indeed decrease the temperature required to start releasing hydrogen in Mg powder, even without the addition of catalysts, as have been reported in numerous studies [71–73].

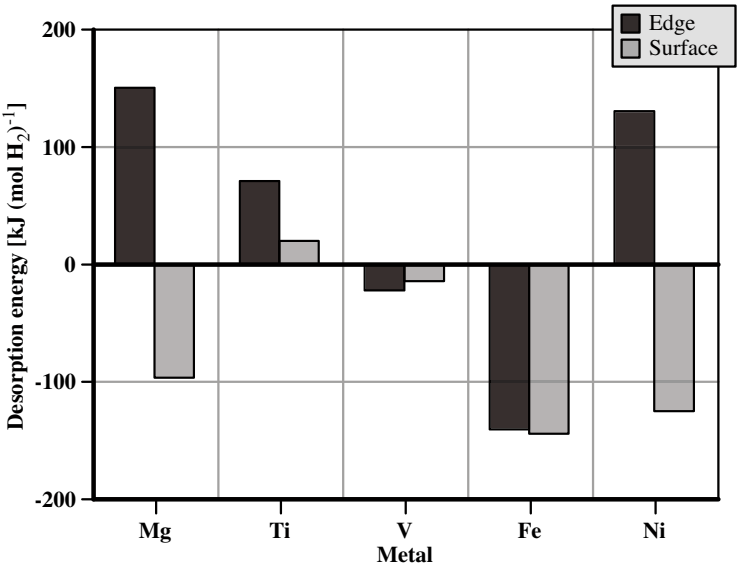

Figure 3.16: Individual hydrogen desorption energies for $Mg_{30}MH_{62}$ clusters at two different surface sites. Note that some sites are inherently unstable.

With catalysts present, the hydrogen removal energies are decreased when Ti replaces one Mg, although they are still endothermic. For V, removal of H from both sites are slightly exothermic. The most notable cases, however, are Fe and Ni. For Fe, the removal energies of H atoms from both the edge and surface Fe sites are strongly negative, so is removal from the Ni surface site. In other words, the surface sites are unstable, which should be beneficial for hydrogen desorption. Ultimately, though, the speed of this reaction at ambient conditions also depends on a favorable activation energy.

The Fe doped MgH_2 system was chosen for a detailed study to see how it evolves as hydrogen atoms are successively removed. As the geometry was re-optimized following the removal of the first hydrogen atom from the *edge* site (Fig. 3.17A), the iron atom attracted another hydrogen from the center of the cluster to replace the removed hydrogen and preserve the tetrahedral coordination (Fig. 3.17B). The ability of the iron atom to attract nearby hydrogen atoms remains after removing another nearby hydrogen (Fig. 3.17C), and also after removing two more hydrogen atoms simultaneously (Fig. 3.17D). After two hydrogens had been removed (Fig. 3.17C), the final structure changed into an arrangement with one *extra* hydrogen atom being close to iron. The most interesting observation, however, was that when two out of these five hydrogen atoms were removed, and the structure re-optimized, a FeH_4 tetrahedral arrangement reformed, via a displacement of the Fe atom towards the hydrogen-rich core of the cluster. It thus appears that the Fe atom follows the MgH_2/Mg interface during dehydrogenation in its search for hydrogen atoms.

The ability of Fe atoms on the Mg cluster surface to coordinate and attract hydrogen seems to confirm the "gateway" mechanism, but with the additional

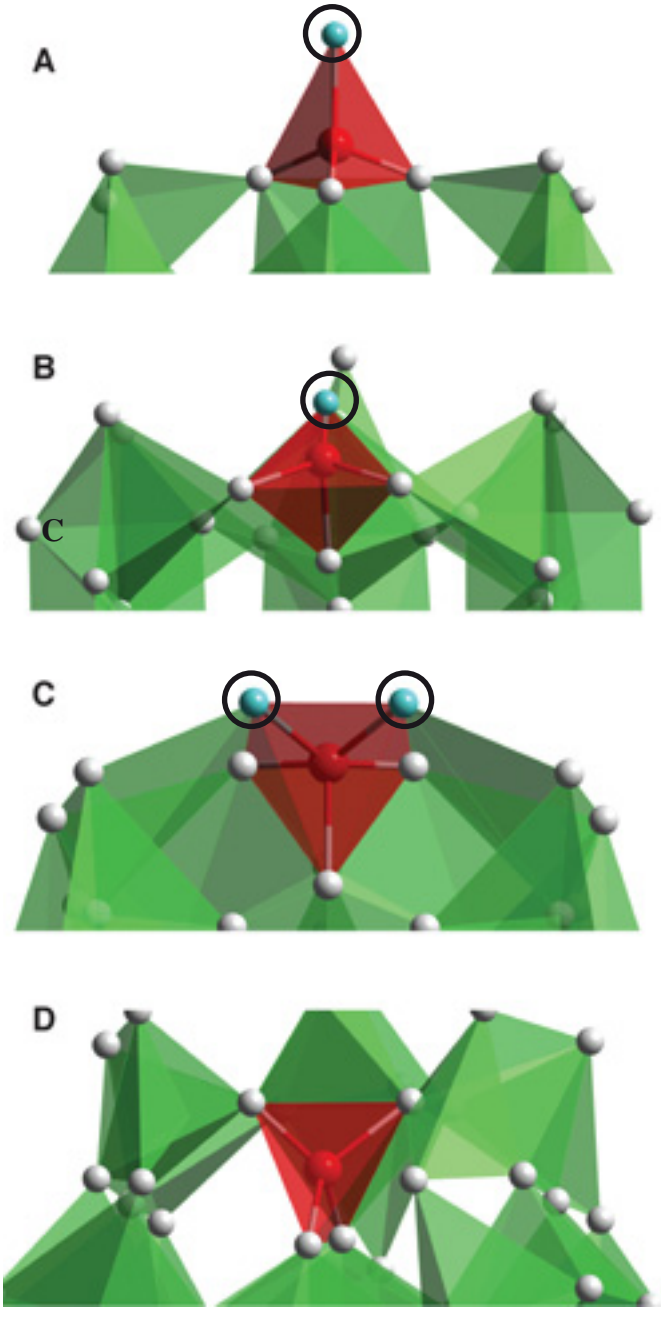

Figure 3.17: Successive dehydrogenation from an Fe atom. At each step, the encircled hydrogen atom(s) are removed and the structure reoptimized. **A**: $Mg_{30}Fe\text{-}H_{62}$. Fe binds four hydrogen atoms tetrahedrally. **B**: $Mg_{30}Fe\text{-}H_{61}$. Tetrahedral coordination reformed after H removal and optimization. **C**: $Mg_{30}Fe\text{-}H_{60}$. Fe now binds five H atoms. **D**: $Mg_{30}Fe\text{-}H_{58}$. Fe becomes tetrahedrally coordinated once again.

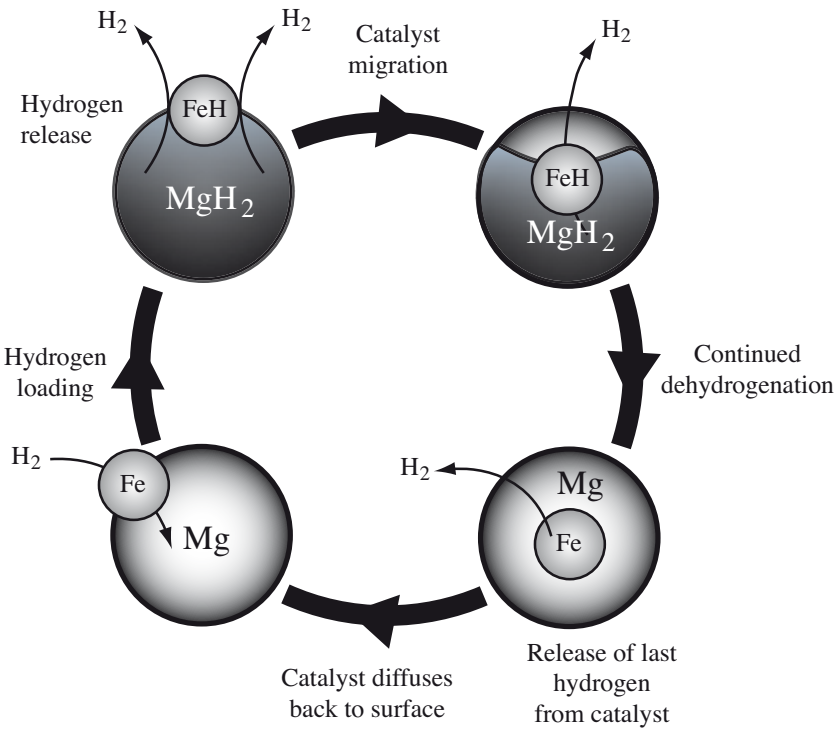

Figure 3.18: Outline of the proposed gateway+migration mechanism.

feature that Fe catalysts migrate below the surface, continuously catalyzing the release of hydrogen. We call this the "Gateway+Migration" mechanism. It is outlined in Fig. 3.18. This way of catalysis is similar to the "zipper" mechanism proposed for $NaAlH_4$ [74].

Conclusions & Outlook

Several cathode materials where investigated from an electrochemical and structural point of view. The crystal structure of Li_2FeSiO_4 is now much better understood. It was hoped that manganese substitution would be enough to increase the capacity of this cathode material, but the findings here, together with other experimental results, suggests that manganese substitution alone will not be enough.

A new criterion for catalyst selection in carbon nanotube growth has been presented. It is based on the idea that strong adhesion between SWNTs and the metal surfaces from which they grow is a necessary (but not sufficient) requirement for SWNT growth at equilibrium conditions. The first principles calculations show that this condition is fulfilled by the commonly used metals Fe, Co and Ni, but not by Cu, Pd and Au. The theory was tested experimentally for Mo and Cu particles and found to be in good agreement.

The concept of transition metal catalysis of hydrogen release from magnesium powders was well-known, but the exact mechanism unclear. It has been proposed that there is a gateway mechanism of catalysis, whereby the transition metal particles shuttles hydrogen atom to the surface. This phenomenon was observed at atomic scale in the DFT calculations performed on Mg/MgH_2 clusters, which thereby confirms the hypothesis.

Possible topics that would be worthwhile to study further include:

- Ab initio molecular dynamics simulations of the cathode materials involved. The aim would be to estimate activation energies of diffusion, and stability of different partially lithiated phases. Phonon calculations would also be useful in that regard.
- The performance of hybrid functionals incorporating exact exchange for cathode materials, especially in prediction of intercalation voltages.
- Applying advanced structural search methods, such as random search and metadynamics, to determine phases of cathode materials, especially delithiated ones.
- The influence of curvature and surface features such as facets and steps on SWNT-metal interaction strength.
- Ab initio calculations of carbon-metal binding strengths of a wider range of catalytic metals and alloys to determining binding strengths and look for chiral selectivity.
- Developing improved semi-empirical models based on the properties calculated in the previous point.

- Confirming the semi-empirical MD simulations of SWNT growth with ab initio MD. This is extremely challenging, but might be possible with future computer systems.
- It would be interesting to study bigger MgH_2 clusters, with say, 10 atom transition metal clusters as catalysts, especially with ab initio molecular dynamics.
- For MgH_2 to release hydrogen at much lower temperatures, one has to come up with ways to destabilize the material. The most promising approach would be mixing with other hydrides, while still maintaining the other good technical properties of MgH_2.
- Many potential hydrogen storage materials are studied ab initio at the bulk level, even though they are always used as nanopowders in practical use. So there are probably many other metal hydrides where cluster and surface properties should be investigated ab initio.

Acknowledgements

First, I would like to thank my supervisor Rajeev Ahuja. He gave me the opportunity to do my PhD studies in this outstanding research group and got me involved in so many interesting research projects. Acknowledgement goes to him and the other seniors of our group Börje Johansson, Olle Eriksson, Lars Nordström and Peter Oppeneer for getting all these incredibly bright people together. I am grateful for the nice and creative atmosphere. Many thanks to all the people in the DMT group for interesting discussions.

I have to especially mention Moysés for our great collaboration on the cluster study, and for always being there to explain the trickier points of physics. His command of everything physics is truly astonishing. And thank you Torbjörn for tutoring me in the RSPt code, and for many long discussions about programming and the inner workings of ab initio programs in general. My former office mate Duck-Young Kim for many rewarding discussions of physics and everyday computational problems. And all the people in Å13212 for never turning down a chat or a coffee break when I didn't feel like working.

I would like to thank all the other co-authors and collaborators in the projects: "Josh" Thomas, Anti Liivat, Anton Nytén, Arne Rosén, Kim Bolton, Feng Ding, Haiming Duan, Jakub Baran, Puru Jena, and especially Andreas Larsson, who has been my de facto second supervisor. I think we all managed to put together some nice teamwork despite being spread all over the world. We never gave up, despite all the complications we ran into at different stages of the projects, and in the end, it payed off.

Thanks especially to Moysés Araújo, Andreas Blomqvist, and Andreas Larsson for critical reading of the thesis.

I appreciate all the work put in by former system administrators Lars(B), Weine, Thomas Dziekan, and the late Anders Ekström to keep the group's local computers running and precious research data safe.

I must also mention my (physics) master thesis supervisor Erik Sjöqvist and the people in the quantum chemistry group. Thanks for getting me into theoretical physics and computational chemistry in the first place.

Most of the calculations would not have been possible to do without allocations at the Swedish National Supercomputing Centers. I am especially grateful for extra computer time allocations at the Uppsala Multidisciplinary Center for Advanced Computational Science (UPPMAX).

Finally, I also thank my family and friends for their support, patience and encouragement.

Summary in Swedish

I denna avhandling har *ab initio*-beräkningar använts för att utforska egenskaper hos ett antal material med koppling till energi- och nanoteknologiska tillämpningar. Avhandlingen består av två delar. I första delen belyses de teoretiska metoder som använts för beräkningarna, medan andra delen innehåller sammanfattningar av de artiklar som ingår. De första tre artiklarna (I-III) är relaterade till katodmaterial för uppladdningsbara batterier. Artiklarna IV-VII behandlar tillväxt av kolnanorör, med specifikt fokus på katalys och kolnanorörens interaktion med metallkluster. Den sista artikeln (VIII) undersöker vätefrisättning i magnesiumhydridkluster och hur den påverkas av närvaron av övergångsmetaller.

I studierna av uppladdningsbara batterier har målet varit att karaktärisera nya, alternativa, katodmaterial med avseende på kristallstruktur och elektrokemiska egenskaper. Sett ur ett metodutvecklingsperspektiv var det också viktigt att jämföra utfallet av de teoretiska beräkningarna med experimentella mätningar, i de fall de fanns, för att bilda sig en uppfattning om existerande metoder såsom täthetsfunktionalteori har tillräcklig noggrannhet för kunna modellera materialen. Artikel I handlar om litiumjärnsilikat, ett katodmaterial, som i likhet med den annars populära litiumjärnfosfaten, bygger på redoxreaktioner med järn istället för den dyra kobolten, som ofta används i dagens litiumjonbatterier med koboltoxid. Beräkningarna visar på förändringar i kristallstrukturen, jämfört med den experimentellt bestämda geometrin. Man kan också se att det existerar flera olika faser av det halvt urladdade materialet, som antagligen inte kan samexistera vid rumstemperatur. I artikel II undersöks samma material, men med 12.5% mangan inblandat istället för järn. Syfte är att öka materials energikapacitet, eftersom mangan kan oxideras till högre oxidationstal än järn. Tyvärr tyder beräkningarna på att strukturell instabilitet uppträder även vid denna förhållandevis låga koncentration. Den nödvändiga potentialen för att ladda ur katoden till mer än 50% var också för hög (4.7-4.8V) för att vara praktiskt användbar.

Arbetet kring kolnanorör har syftat till att förstå de kemiska reaktionerna som styr tillväxten av nanotuber under själva syntesen. Metallpartiklar används alltid som katalysatorer vid produktion av kolnanorör, och fokus har varit på hur kolnanorör interagerar med dessa metallpartiklar. I artikel IV redovisas en förstudie om vilka modeller som är lämpliga att använda för att beräkna bindningsenergi mellan kolnanoröret och metallytan på ett kluster. Det viktigaste resultatet var att bara använda en enstaka metallatom som sub-

stitut för metallytan inte är tillräckligt för att kunna beräkna tillförlitliga bindingsenergier. Istället måste åtminstone en ringstruktur av metallatomer användas som modell för att man ska erhålla korrekta trender och rätt storleksordning på bindingsenergin.

Med en bättre insikt om lämpliga modeller fortsätter arbetet i artikel V med att jämföra bindingsenergierna mellan två grupper av metaller: katalytiska aktiva metaller som järn, kobolt och nickel, versus, i andra sammanhang, traditionellt använda katalytiska metaller såsom palladium, koppar och guld. Slutsatsen av studien är att katalytiskt aktiva metaller delar en viktig egenskap, nämligen att bindingsenergin till kolnanorören är "lagom" stark. I artikeln presenteras teorin att det beror på att optimala interaktionen mellan kolnanorör och metallkluster uppkommer som svar på en balans mellan två krafter, dels måste metallbindningen vara tillräckligt stark för att kunna stabilisera de grafitstrukturer som bildas på ytan samt hindra att nanorören inte lossnar från partikel under tillväxt, men den kan inte heller vara så stark att metallkarbider bildas istället kolnanostrukturer. Denna teori testas sedan experimentellt i artikel VI, där katalytiska partiklar bestående av en blandning av koppar och molybden används. Varken koppar eller molybden kunde ensamt katalysera tillväxt. Koppar kan inte bryta ned gasen som används som kolkälla, och molybden bildar stabil molybdenkarbid istället för kolnanostrukturer. Endast en blandning av koppar och molybden fungerar tillfredsställande som katalysator, vilket bekräftar teorin om optimal bindingsenergi.

I det sista arbetet om kolnanorör (artikel VII) undersöks hur villkoren ser ut för att uppnå kiralitetsselektiv tillväxt av nanorör. Slutsatsen från undersökningen är att tillväxtprocesser där nanorören växer ut från själva metallytan, till exempel genom plantering av kolhemisfärer på en yta, eller genom att bara designa själva ytan i sig, sannolikt inte kommer att fungera med enbart termodynamisk kontroll, beroende på de små energiskillnaderna mellan korta fragment av växande nanorör. Istället föreslås ett tillvägagångssätt där man utnyttjar den mycket större skillnaden i stabilitet mellan kolnanorör med icke-terminerade ändar, dvs när de inte är bundna till en metallyta.

Utöver studierna av kolnanorör och katodmaterial ingår även en artikel (VIII) om vätefrisättning i magnesiumhydridkluster, och hur den påverkas av närvaron av övergångsmetaller. Magnesiumhydrid är ett klassiskt material för lagra väte i kemisk form, dvs bundet inuti ett annat material. Det är känt sedan tidigare att tillsatser av små mängder övergångsmetaller avsevärt ökar frisättningshastigheten av väte från magnesiumpulver. I artikeln demonstreras det hur metallerna titan, vanadin, järn och nickel, inte bara sänker dissociationsenergin för väte, utan även hur övergångsmetaller attraherar väteatomer på ytan och inuti materialet. Genom att studera strukturrelaxationer i klustren kan man se hur t.ex. järnatomer migrerar från ytan mot centrum av klustret för att binda nya väten, som sedan dissocieras från järnatomen med en lägre energi än i det odopade materialet.

Bibliography

[1] P. Hohenberg and W. Kohn. Inhomogeneous electron gas. *Phys. Rev.*, 136(3B):B864–B871, Nov 1964.

[2] W. Kohn and L. J. Sham. Self-consistent equations including exchange and correlation effects. *Phys. Rev.*, 140(4A):A1133–A1138, Nov 1965.

[3] Lars Hedin. New method for calculating the one-particle green's function with application to the electron-gas problem. *Phys. Rev.*, 139(3A):A796–A823, Aug 1965.

[4] G. Kresse and J. Hafner. Ab initio molecular dynamics for liquid metals. *Phys. Rev. B*, 47:558, 1993.

[5] G. Kresse and J. Hafner. Ab initio molecular-dynamics simulation of the liquid-metal-amorphous-semiconductor transition in germanium. *Phys. Rev. B*, 49:14251, 1994.

[6] G. Kresse and J. Furthmüller. Efficiency of ab-initio total energy calculations for metals and semiconductors using a plane-wave basis set. *Comput. Mat. Sci.*, 6:15, 1996.

[7] G. Kresse and J. Furthmüller. Efficient iterative schemes for ab initio total-energy calculations using a plane-wave basis set. *Phys. Rev. B*, 54:11169, 1996.

[8] G. Kresse and D. Joubert. From ultrasoft pseudopotentials to the projector augmented-wave method. *Phys. Rev. B*, 59:1758, 1999.

[9] R.J. Needs, M.D. Towler, N.D. Drummond, and P. López Ríos. *CASINO version 2.3 User Manual*. Cambridge University, Cambridge, 2008.

[10] J. P. Perdew, K. Burke, and M. Ernzerhof. Generalized gradient approximation made simple. *Phys. Rev. Lett.*, 77:3865, 1996.

[11] J. P. Perdew, K. Burke, and M. Ernzerhof. Erratum: Generalized gradient approximation made simple. *Phys. Rev. Lett.*, 78:1396, 1997.

[12] Xin Xu, Qingsong Zhang, Richard P. Muller, and William A. Goddard III. An extended hybrid density functional (X3LYP) with improved descriptions of nonbond interactions and thermodynamic properties of molecular systems. *The Journal of Chemical Physics*, 122(1):014105, 2005.

[13] B. Delley. Ground-state enthalpies: Evaluation of electronic structure approaches with emphasis on the density functional method. *Journal of Physical Chemistry A*, 110(50):13632–13639, 2006.

[14] J. L. Rodríguez-López, F. Aguilera-Granja, K. Michaelian, and A. Vega. Structure and magnetism of cobalt clusters. *Phys. Rev. B*, 67(17):174413, May 2003.

[15] Pavel V. Avramov, Konstantin N. Kudin, and Gustavo E. Scuseria. Single wall carbon nanotubes density of states: comparison of experiment and theory. *Chemical Physics Letters*, 370(5-6):597–601, 2003.

[16] E. G. Noya, R. C. Longo, and L. J. Gallego. Density-functional calculations of the structures, binding energies, and spin multiplicities of Fe–C clusters. *The Journal of Chemical Physics*, 119(21):11130–11134, 2003.

[17] Demeter Tzeli and Aristides Mavridis. Theoretical investigation of iron carbide, FeC. *The Journal of Chemical Physics*, 116(12):4901–4921, 2002.

[18] M. Y. Chou and Marvin L. Cohen. Ab initio study of the structural properties of magnesium. *Solid State Communications*, 57(10):785 – 788, 1986.

[19] Renata M. Wentzcovitch and Marvin L. Cohen. Theoretical model for the hcp-bcc transition in Mg. *Phys. Rev. B*, 37(10):5571–5576, Apr 1988.

[20] J. D. Althoff, P. B. Allen, R. M. Wentzcovitch, and John A. Moriarty. Phase diagram and thermodynamic properties of solid magnesium in the quasiharmonic approximation. *Phys. Rev. B*, 48(18):13253–13260, Nov 1993.

[21] S. Mehta, G. D. Price, and D. Alfè. Ab initio thermodynamics and phase diagram of solid magnesium: A comparison of the LDA and GGA. *The Journal of Chemical Physics*, 125(19):194507, 2006.

[22] Y Song, ZX Guo, and R Yang. Influence of titanium on the hydrogen storage characteristics of magnesium hydride: a first principles investigation. *Materials Science and Engineering A*, 365(1-2):73–79, JAN 25 2004. 1st International Conference on Multiscale Materials Modelling (MMM), LONDON, ENGLAND, JUN 17-22, 2002.

[23] D Chen, YM Wang, L Chen, S Liu, CX Ma, and LB Wang. Alloying effects of transition metals on chemical bonding in magnesium hydride MgH_2. *ACTA MATERIALIA*, 52(2):521–528, JAN 19 2004.

[24] Y Song, ZX Guo, and R Yang. Influence of selected alloying elements on the stability of magnesium dihydride for hydrogen storage applications: A first-principles investigation. *Physical Review B*, 69(9), MAR 2004.

[25] Sudhakar V. Alapati, J. Karl Johnson, and David S. Sholl. Using first principles calculations to identify new destabilized metal hydride reactions for reversible hydrogen storage. *Physical Chemistry Chemical Physics*, 9(12):1438–1452, 2007.

[26] M. Born and K. Huang. *Dynamical Theory of Crystal Lattices*. Oxford University Press, 1956.

[27] R. G. Woolley. Quantum chemistry beyond the Born-Oppenheimer approximation. *Journal of Molecular Structure (Theochem)*, 230:17, 1991.

[28] Michele Lazzeri, A. Marco Saitta, and Francesco Mauri. Breakdown of the adiabatic approximation in a doped graphene monolayer and in metallic carbon nanotubes. *Physica Status Solidi (b)*, 244(11):4118, 2007.

[29] Simone Pisana, Michele Lazzeri, Cinzia Casiraghi, Kostya S. Novoselov, A. K. Geim, Andrea C. Ferrari, and Francesco Mauri. Breakdown of the adiabatic Born-Oppenheimer approximation in graphene. *Nature Materials*, 6:198, 2007.

[30] Jan M. L. Martin and Glênisson de Oliveira. Towards standard methods for benchmark quality ab initio thermochemistry—W1 and W2 theory. *The Journal of Chemical Physics*, 111(5):1843–1856, 1999.

[31] A. Daniel Boese, Mikhal Oren, Onur Atasoylu, Jan M. L. Martin, Mihály Kállay, and Jürgen Gauss. W3 theory: Robust computational thermochemistry in the kJ/mol accuracy range. *The Journal of Chemical Physics*, 120(9):4129–4141, 2004.

[32] Amir Karton, Elena Rabinovich, Jan M. L. Martin, and Branko Ruscic. W4 theory for computational thermochemistry: In pursuit of confident sub-kJ/mol predictions. *The Journal of Chemical Physics*, 125(14):144108, 2006.

[33] Stefano de Gironcoli. Lattice dynamics of metals from density-functional perturbation theory. *Phys. Rev. B*, 51(10):6773–6776, Mar 1995.

[34] Andrea Dal Corso and Stefano de Gironcoli. Ab initio phonon dispersions of Fe and Ni. *Phys. Rev. B*, 62(1):273–277, Jul 2000.

[35] Nicholas C. Handy, Yukio Yamaguchi, and Henry F. Schaefer III. The diagonal correction to the Born–Oppenheimer approximation: Its effect on the singlet–triplet splitting of CH_2 and other molecular effects. *The Journal of Chemical Physics*, 84(8):4481–4484, 1986.

[36] Jürgen Gauss, Attila Tajti, Mihály Kállay, John F. Stanton, and Péter G. Szalay. Analytic calculation of the diagonal Born-Oppenheimer correction within configuration-interaction and coupled-cluster theory. *The Journal of Chemical Physics*, 125(14):144111, 2006.

[37] Werner Kutzelnigg. The adiabatic approximation I. The physical background of the Born-Handy ansatz. *Molecular Physics*, 90:909, 1997.

[38] Mauricio Cafiero and Ludwik Adamowicz. Non-Born-Oppenheimer calculations of the ground state of H_3. *International Journal of Quantum Chemistry*, 107:2679, 2007.

[39] J.P. Perdew, J.A. Chevary, S.H. Vosko, K.A. Jackson, M.R. Pederson, D.J. Singh, and C. Fiolhais. Atoms, molecules, solids, and surfaces: Applications of the generalized gradient approximation for exchange and correlation. *Phys. Rev. B*, 46:6671, 1992.

[40] J.P. Perdew, J.A. Chevary, S.H. Vosko, K.A. Jackson, M.R. Pederson, D.J. Singh, and C. Fiolhais. Erratum: Atoms, molecules, solids, and surfaces: Applications of the generalized gradient approximation for exchange and correlation. *Phys. Rev. B*, 48:4978, 1993.

[41] Filipp Furche and John P. Perdew. The performance of semilocal and hybrid density functionals in 3d transition-metal chemistry. *The Journal of Chemical Physics*, 124(4):044103, 2006.

[42] Jianmin Tao, John P. Perdew, Viktor N. Staroverov, and Gustavo E. Scuseria. Climbing the density functional ladder: Nonempirical meta–generalized gradient approximation designed for molecules and solids. *Phys. Rev. Lett.*, 91(14):146401, Sep 2003.

[43] R. Armiento and A. E. Mattsson. Functional designed to include surface effects in self-consistent density functional theory. *Phys. Rev. B*, 72(8):085108, Aug 2005.

[44] P. E. Blöchl. Projector augmented-wave method. *Phys. Rev. B*, 50(24):17953–17979, Dec 1994.

[45] P. E. Blöchl, Clemens J. Först, and Johannes Schimpl. The projector augmented wave metod: ab-initio molecular dynamics with full wave functions. *arXiv:cond-mat*, page 0201015v2, 2008.

[46] D D Koelling and B N Harmon. A technique for relativistic spin-polarised calculations. *Journal of Physics C: Solid State Physics*, 10(16):3107–3114, 1977.

[47] N. A. W. Holzwarth, G. E. Matthews, R. B. Dunning, A. R. Tackett, and Y. Zeng. Comparison of the projector augmented-wave, pseudopotential, and linearized

augmented-plane-wave formalisms for density-functional calculations of solids. *Phys. Rev. B*, 55(4):2005–2017, Jan 1997.

[48] Andreas Köhn, Florian Weigend, and Reinhart Ahlrichs. Theoretical study on clusters of magnesium. *Physical Chemistry Chemical Physics*, 3(5):711–719, 2001.

[49] Karin Eichkorn, Oliver Treutler, Holger Öhm, Marco Häser, and Reinhart Ahlrichs. Auxiliary basis sets to approximate coulomb potentials. *Chemical Physics Letters*, 240(4):283 – 289, 1995.

[50] Cristian V. Diaconu, Art E. Cho, J. D. Doll, and David L. Freeman. Broken-symmetry unrestricted hybrid density functional calculations on nickel dimer and nickel hydride. *The Journal of Chemical Physics*, 121(20):10026–10040, 2004.

[51] Oliver Treutler and Reinhart Ahlrichs. Efficient molecular numerical integration schemes. *The Journal of Chemical Physics*, 102(1):346–354, 1994.

[52] Malte von Arnim and Reinhart Ahlrichs. Geometry optimization in generalized natural internal coordinates. *The Journal of Chemical Physics*, 111(20):9183–9190, 1999.

[53] Anton Nytén, Ali Abouimrane, Michel Armand, Torbjörn Gustafsson, and John O. Thomas. Electrochemical performance of Li_2FeSiO_4 as a new Li-battery cathode material. *Electrochemistry Communications*, 7(2):156 – 160, 2005.

[54] Anton Nytén, Marten Stjerndahl, Håkan Rensmo, Hans Siegbahn, Michel Armand, Torbjörn Gustafsson, Kristina Edström, and John O. Thomas. Surface characterization and stability phenomena in Li_2FeSiO_4 studied by PES/XPS. *Journal of Materials Chemistry*, 16(34):3483–3488, 2006.

[55] Shin-ichi Nishimura, Shogo Hayase, Ryoji Kanno, Masatomo Yashima, Noriaki Nakayama, and Atsuo Yamada. Structure of Li_2FeSiO_4. *Journal of the American Chemical Society*, 130(40):13212–13213, 2008.

[56] Sen Zhang, Chao Deng, and Saiyu Yang. Preparation of nano-Li_2FeSiO_4 as cathode material for lithium-ion batteries. *Electrochemical and Solid-State Letters*, 12(7):A136–A139, 2009.

[57] R. Dominko, M. Bele, M. Gaberscek, A. Meden, M. Remskar, and J. Jamnik. Structure and electrochemical performance of Li_2MnSiO_4 and Li_2FeSiO_4 as potential Li-battery cathode materials. *Electrochemistry Communications*, 8(2):217 – 222, 2006.

[58] Anton Kokalj, Robert Dominko, Gregor Mali, Anton Meden, Miran Gaberscek, and Janez Jamnik. Beyond one-electron reaction in Li cathode materials: Designing $Li_2Mn_xFe_{1-x}SiO_4$. *Chemistry of Materials*, 19(15):3633–3640, 06 2007.

[59] R. Dominko. Li_2MSiO_4 (M=Fe and/or Mn) cathode materials. *Journal of Power Sources*, 184(2):462 – 468, 2008.

[60] Anton Nytén, Saeed Kamali, Lennart Haggstrom, Torbjörn Gustafsson, and John O. Thomas. The lithium extraction/insertion mechanism in Li_2FeSiO_4. *Journal of Materials Chemistry*, 16(23):2266–2272, 2006.

[61] B. L. Ellis, W. R. M. Makahnouk, Y. Makimura, K. Toghill, and L. F. Nazar. A multifunctional 3.5 V iron-based phosphate cathode for rechargeable batteries. *Nat Mater*, 6(10):749–753, 10 2007.

[62] Oleg V. Yazyev and Alfredo Pasquarello. Effect of metal elements in catalytic growth of carbon nanotubes. *Physical Review Letters*, 100(15):156102, 2008.

[63] D. Takagi, Y. Homma, H. Hibino, S. Suzuki, and Y. Kobayashi. Single-walled carbon nanotube growth from highly activated metal nanoparticles. *Nano Letters*, 6(12):2642–2645, 2006.

[64] Daisuke Takagi, Yoshihiro Kobayashi, Hiroki Hibino, Satoru Suzuki, and Yoshikazu Homma. Mechanism of gold-catalyzed carbon material growth. *Nano Letters*, 8(3):832–835, 2008.

[65] R.T.K. Baker. Catalytic growth of carbon filaments. *Carbon*, 27(3):315 – 323, 1989.

[66] Wojciech Grochala and Peter P. Edwards. Thermal decomposition of the non-interstitial hydrides for the storage and production of hydrogen. *Chemical Reviews*, 104(3):1283–1316, 02 2004.

[67] Vincent Bérubé, Gregg Radtke, Mildred Dresselhaus, and Gang Chen. Size effects on the hydrogen storage properties of nanostructured metal hydrides: A review. *International Journal of Energy Research*, 31(6-7):637–663, 2007.

[68] J. F. Pelletier, J. Huot, M. Sutton, R. Schulz, A. R. Sandy, L. B. Lurio, and S. G. J. Mochrie. Hydrogen desorption mechanism in MgH_2-Nb nanocomposites. *Phys. Rev. B*, 63(5):052103, Jan 2001.

[69] Rudy W. P. Wagemans, Joop H. van Lenthe, Petra E. de Jongh, A. Jos van Dillen, and Krijn P. de Jong. Hydrogen storage in magnesium clusters: Quantum chemical study. *Journal of the American Chemical Society*, 127(47):16675–16680, 11 2005.

[70] L. H. Liang, G. W. Yang, and Baowen Li. Size-dependent formation enthalpy of nanocompounds. *The Journal of Physical Chemistry B*, 109(33):16081–16083, 07 2005.

[71] A. Zaluska, L. Zaluski, and J. O. Ström-Olsen. Nanocrystalline magnesium for hydrogen storage. *Journal of Alloys and Compounds*, 288(1-2):217 – 225, 1999.

[72] Nobuko Hanada, Takayuki Ichikawa, Shin-Ichi Orimo, and Hironobu Fujii. Correlation between hydrogen storage properties and structural characteristics in mechanically milled magnesium hydride MgH_2. *Journal of Alloys and Compounds*, 366(1-2):269 – 273, 2004.

[73] Nobuko Hanada, Takayuki Ichikawa, and Hironobu Fujii. Catalytic effect of nanoparticle 3d-transition metals on hydrogen storage properties in magnesium hydride MgH_2 prepared by mechanical milling. *The Journal of Physical Chemistry B*, 109(15):7188–7194, 03 2005.

[74] Ali Marashdeh, Roar A. Olsen, Ole Martin Løvvik, and Geert-Jan Kroes. A density functional theory study of Ti-doped $NaAlH_4$ clusters. *Chemical Physics Letters*, 426(1-3):180 – 186, 2006.

Acta Universitatis Upsaliensis

Digital Comprehensive Summaries of Uppsala Dissertations from the Faculty of Science and Technology 670

Editor: The Dean of the Faculty of Science and Technology

A doctoral dissertation from the Faculty of Science and Technology, Uppsala University, is usually a summary of a number of papers. A few copies of the complete dissertation are kept at major Swedish research libraries, while the summary alone is distributed internationally through the series Digital Comprehensive Summaries of Uppsala Dissertations from the Faculty of Science and Technology. (Prior to January, 2005, the series was published under the title "Comprehensive Summaries of Uppsala Dissertations from the Faculty of Science and Technology".)

Distribution: publications.uu.se
urn:nbn:se:uu:diva-108261

ACTA
UNIVERSITATIS
UPSALIENSIS
UPPSALA
2009